

A Heterogeneous Out-of-Equilibrium Nonlinear q -Voter Model with Zealotry

Andrew Mellor,¹ Mauro Mobilia,¹ and R.K.P. Zia^{2,3}

¹*Department of Applied Mathematics, School of Mathematics, University of Leeds, Leeds LS2 9JT, U.K.*

²*Department of Physics & Astronomy, Iowa State University, Ames, IA 50011, USA*

³*Center for Soft Matter and Biological Physics, Department of Physics,
Virginia Polytechnic Institute & State University, Blacksburg, VA 24061, USA*

We study the dynamics of the out-of-equilibrium nonlinear q -voter model with two types of susceptible voters and zealots, introduced in [EPL **113**, 48001 (2016)]. In this model, each individual supports one of two parties and is either a susceptible voter of type q_1 or q_2 , or is an inflexible zealot. At each time step, a q_i -susceptible voter ($i = 1, 2$) consults a group of q_i neighbors and adopts their opinion if all group members agree, while zealots are inflexible and never change their opinion. This model violates detailed balance whenever $q_1 \neq q_2$ and is characterized by two distinct regimes of low and high density of zealotry. Here, by combining analytical and numerical methods, we investigate the non-equilibrium stationary state of the system in terms of its probability distribution, non-vanishing currents and unequal-time two-point correlation functions. We also study the switching times properties of the model by exploiting approximate mappings onto the model of [Phys. Rev. E **92**, 012803 (2015)] that satisfies the detailed balance, and also outline some properties of the model near criticality.

PACS numbers: 89.75.-k, 02.50.-r, 05.40.-a, 89.75.Fb

I. INTRODUCTION

Parsimonious individual-based models have been commonly used to describe collective social phenomena for more than four decades [1]. In particular, statistical physics models have proven especially well-suited to reveal the micro-macro connections in social dynamics and to help reveal the relationships existing between phenomena appearing across disciplines (like biology, ecology, economics) [2]. In particular, the voter model (VM) [3] serves as a reference to describe the evolution of opinions in interacting populations [2, 4]. It is however well established that the VM is built on a number of oversimplified assumptions: For instance, the VM considers that all voters are similar: In the absence of any self-confidence, they change their opinion by imitating neighbors. This mechanism of *conformity by imitation* does not allow to maintain social diversity in the long run, but always leads to a consensus. However, social scientists have shown that the collective dynamics of a society greatly depends on the different responses to stimuli by the members of a society [5–7]. A simple way to accommodate a population with different levels of confidence is simply to assume that some agents are “zealots” and either favor one opinion [8] or inflexibly maintain a fixed opinion [9]. Since the introduction of zealots in the VM, the effect of zealotry has been studied in other models of social dynamics [10] and in various contexts [11].

In this work, we focus on the so-called two-state nonlinear q -voter model (q VM) [12]. In this variant of the VM, that has received much attention recently [13], each voter can be influenced by a group of q neighbors [14] [15]. This mimics the fact that group pressure is known to influence the degree of conformity, especially above a group size threshold [7]. Furthermore, social scientists have shown that conformity via imitation is a driving

mechanism for collective actions that is influenced by the size of social groups, and they also found that conformity can be seriously deflected by individuals (like zealots) that are able to resist group pressure [6, 7]. Motivated by these considerations [5, 6], the basic features of the q VM and zealotry have recently been combined in the q -voter model with inflexible zealots (q VMZ) [16] and in a heterogeneous counterpart model, called the $2q$ VZ, in which two subgroups of susceptible voters interacting with their neighbors with different q ’s: namely, with $q_1 < q_2$ [17].

In the q VMZ and $2q$ VZ, group-size limited conformity and zealotry are accounted for, and zealots significantly tame the level of social conformity in the population [16, 17]. Furthermore, the dynamics of the q VMZ and $2q$ VZ in a well-mixed population is similar and is characterized by two phases as in systems in thermal equilibrium: Below a critical level of zealotry, the opinion distribution transitions from single-peaked becomes bimodal and, in finite populations, the dynamics is characterized by the fluctuation-driven switching between two states [16, 17]. Yet, while the q VMZ of Ref. [16] obeys detailed balance and its stationary distribution can be obtained exactly, this is not the case of the $2q$ VZ even in the simple case of a well-mixed population when the system relaxes into a non-equilibrium steady state (NESS) [17]. The fact that the $2q$ VZ does not obey detailed balance has many important statistical physics consequences: There is generally no simple way to obtain the NESS distribution [18], while persistent probability currents are responsible for subtle oscillations and non-trivial correlation functions [17, 19]. From a social dynamics viewpoint, the composition of the society being very heterogeneous, it would be relevant to consider models with a distribution of q ’s that would reflect different responses to multiple social stimuli [5]. While analytical progress appears to be difficult in such a general

case, much can be learnt about the influence of being out-of-equilibrium on the social dynamics by considering the simple 2qVZ whose detailed analysis is presented here. In particular, we are able to show that susceptible voters with smaller q change their opinion more quickly and drive those in the other subgroup, and directed, yet subtle, *oscillations* associated with fluctuating quantities can be measured [20].

In this work, we therefore focus on the 2qVZ and characterize the properties of its NESS in terms of the master equation, stochastic simulations and continuum approximations based on mean-field and Fokker-Planck equations. While a brief account of some of these features was given in Ref. [17], here we considerably generalize that study and also investigate the switching dynamics of the 2qVZ.

The remainder of this paper is organized as follows: The details of the 2qVZ are specified in the next section, along with the underlying master equation. The microscopic characterization of the NESS in terms of the master equation and relevant observables is addressed in Sec. III. Sec. IV is dedicated to the continuum approximation of the 2qVZ dynamics in terms of mean-field rate equations and through a linear Gaussian approximation (LGA) of the underlying Fokker-Planck equation (for a system of large but finite size) [19, 21, 22]. This allows us to show in some details, how the the LGA offers the best insight into probability currents and their manifestations in the 2qVZ's NESS far from criticality, as explained in Sec. IV.B. In Sec. IV.C, we exploit a Fokker-Planck formulation to shed light on the switching time properties of the 2qVZ via approximate mappings onto the qVMZ whereas the behavior near criticality is briefly discussed in Sec. IV.D. While most examples given in Section IV are concerned with the case of symmetric zealotry (same number of zealots for each party), the generalization to asymmetric zealotry is addressed in Sec. V. We also give a number of analytical and computational details in a series of appendices. We end with a summary, as well as outlook for future research. It is worth noting that while our general analysis applies to any values of q_1 and q_2 , for the sake of simplicity and without loss of generality, the numerical examples reported in our figures have been obtained for $q_{1,2} = 1, 2$.

II. THE 2 q VOTER MODEL WITH ZEALOTRY (2qVZ)

The 2qVZ consists of a population of N voters who hold one of two opinions, denoted by ± 1 . A fraction of the population are inflexible zealots that never change their opinion [9, 16], the number of which are denoted by Z_{\pm} . The remaining population consists of $S = S_1 + S_2$ swing voters of two types, q_1 and q_2 (known as q_i -susceptibles, $i = 1, 2$): S_1 of the swing voters are of type q_1 and there are S_2 swing voters of type q_2 . In our model, the behavior of each voter is fixed, so that Z_{\pm} and S_i are

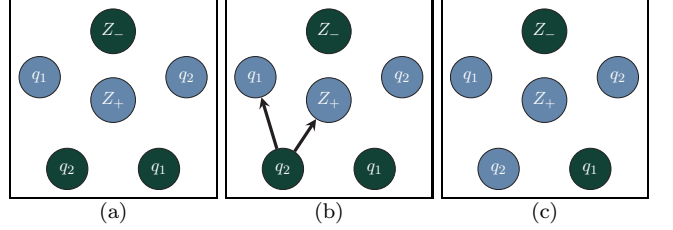


FIG. 1. (Color online). Illustration of the 2qVZ dynamics: (a) the system consists of zealots, q_1 -, and q_2 - susceptibles; each can hold one of two opinions (green/black or blue/grey). (b) A q_i susceptible picks q_i neighbours at random. Here, $q_2 = 2$. (c) If the picked neighbors have same opinion, the focal susceptible voter adopts their opinion, otherwise no change occurs.

conserved, with $S_1 + S_2 + Z_+ + Z_- = N$. As illustrated in Fig. 1, the evolution of the 2qVZ is such that at each update attempt (a) a (focal) voter is chosen at random. (b) If the chosen voter is a zealot then no further action is taken. If the focal voter is a q_i -susceptible is chosen however, then it the opinions of a random group of q_i of its neighbors (repetition is allowed) are collected. (c) If the q_i neighbors have the same opinion that differs from that of the focal voter, the latter adopts the opinion of the group. If there is no consensus within the q_i -group, the opinion of the focal voter does not change. Here, for the sake of simplicity we consider a well-mixed population, i.e. each voter can be thought to as the N nodes of a complete graph and all other voters are “neighbors”.

A. Microscopic Description with a Master Equation

In the absence of explicit spatial structure, the configuration space is a discrete set of $S_1 \times S_2$ points and the system state is completely specified by the pair $\vec{n} := (n_1, n_2)$ where n_i is the number of susceptible voters of type i holding the opinion $+1$. In each update attempt, the system may, or may not, step to one of its four nearest neighboring points. In other words the allowed *changes* are in the set $\{\pm \vec{e}_1, \pm \vec{e}_2\}$, with $\vec{e}_1 := (1, 0)$ and $\vec{e}_2 := (0, 1)$. Thus, we may regard the evolution of the 2qVZ as a two-dimensional random walker with inhomogeneous and biased rates. Such a stochastic process can be readily described by a master equation (ME) for the evolution of $P(\vec{n}, T)$, the probability of finding the system in state \vec{n} after T discrete time steps (or update attempts) from starting in an initial configuration \vec{n}_0 . One of our main interests is in the unique stationary distribution, which has no dependence on the initial configuration \vec{n}_0 , and we can therefore omit any reference to \vec{n}_0 .

For any discrete Markov process, the ME can be written as

$$P(\vec{n}', T+1) = \sum_{\vec{n}} \mathcal{G}(\vec{n}', \vec{n}) P(\vec{n}, T) \quad (1)$$

where \mathcal{G} is known as the transition matrix, or evolution operator. In our case, since $\vec{n}' \in \{\vec{n}, \vec{n} \pm \vec{e}_1, \vec{n} \pm \vec{e}_2\}$, so that, an explicit form for \mathcal{G} is

$$\begin{aligned} \mathcal{G}(\vec{n}', \vec{n}) &= \delta(n'_1, n_1) \delta(n'_2, n_2) W^0(\vec{n}) \\ &+ \sum_{i=1,2, j \neq i} \delta(n'_i, n_i + 1) \delta(n'_j, n_j) W_i^+(\vec{n}) \\ &+ \sum_{i=1,2, j \neq i} \delta(n'_i, n_i - 1) \delta(n'_j, n_j) W_i^-(\vec{n}) \end{aligned} \quad (2)$$

Here, $W^0(\vec{n})$ represents the probability for the system to remain unchanged, while $W_1^\pm(\vec{n})$ and $W_2^\pm(\vec{n})$ stand for the stepping probabilities associated with $\vec{n} \rightarrow \vec{n} \pm \vec{e}_1$ and $\vec{n} \rightarrow \vec{n} \pm \vec{e}_2$, respectively. Explicitly [23], these are

$$\begin{aligned} W_i^+(\vec{n}) &= \frac{S_i - n_i}{N} \left(\frac{M}{N-1} \right)^{q_i} \\ W_i^-(\vec{n}) &= \frac{n_i}{N} \left(\frac{N-M}{N-1} \right)^{q_i} \end{aligned} \quad (3)$$

$$W^0(\vec{n}) = 1 - W_1^+(\vec{n}) - W_1^-(\vec{n}) - W_2^+(\vec{n}) - W_2^-(\vec{n}),$$

where $M = Z_+ + n_1 + n_2$ is the total number of +1 voters before the update. (See (A2) in Appendix A for further details.)

Subsequently, we will be interested in the joint probability,

$$\mathcal{P}(\vec{n}', T'; \vec{n}, T) = \mathcal{G}^{T' - T}(\vec{n}', \vec{n}) P(\vec{n}, T), \quad (4)$$

for finding the system being in a state \vec{n}' at (a later, assuming $T' > T$) time T' and being in state \vec{n} at time T (see (A5)). With these probability distributions, we can compute physical observables such as the average number of q_i voters holding opinion +1 at time T and two-point correlation functions at general times:

$$\begin{aligned} \langle n_i \rangle_T &= \sum_{\vec{n}} n_i P(\vec{n}, T) \\ \langle n'_i n_j \rangle_{T', T} &= \sum_{\vec{n}, \vec{n}'} n'_i n_j \mathcal{P}(\vec{n}', T'; \vec{n}, T). \end{aligned}$$

One quantity of particular interest for the study of the $2qVZ$ is the *net probability current*, given by $\vec{K}(\vec{n}; T) = (K_1, K_2)$, see (A3) in Appendix A. Here, $K_i(\vec{n}; T) = W_i^+(\vec{n})P(\vec{n}; T) - W_i^-(\vec{n})P(\vec{n}'; T)$ denotes the net flow (of probability) from \vec{n} to $\vec{n}' \equiv \vec{n} + \vec{e}_i$, with $i = 1, 2$, $\vec{e}_1 = (1, 0)$ and $\vec{e}_2 = (0, 1)$.

B. Violation of Detailed Balance

In Ref. [17], we emphasized a distinctive feature of the $2qVZ$, namely, that its dynamics is a genuine out-of-equilibrium type, contrary to the $qVMZ$ [16] model. Hence, detailed balance and time reversal symmetry are violated in the $2qVZ$. To establish this fact, we apply

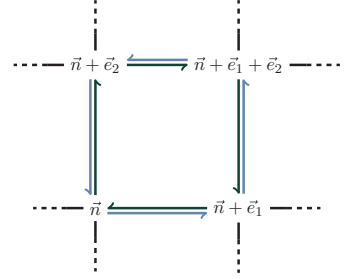


FIG. 2. (Color online). The state space of the $2qVZ$ is of size $(S_1+1) \times (S_2+1)$ and can be represented as a two-dimensional lattice. The probability of traversing the shown loop clockwise (blue/grey) does not equal the probability of traversing in the opposite direction (green/black). By Kolmogorov's criterion, the detailed balance is violated, see text.

the Kolmogorov criterion (A6) [24] on a closed loop consisting of the four \vec{n} 's around a square: $\vec{n} \rightarrow \vec{n} + \vec{e}_1 \rightarrow \vec{n} + \vec{e}_1 + \vec{e}_2 \rightarrow \vec{n} + \vec{e}_2 \rightarrow \vec{n}$, illustrated in Fig. 2. The product of transition probabilities around this loop is

$$W_1^+(\vec{n}) W_2^+(\vec{n} + \vec{e}_1) W_1^-(\vec{n} + \vec{e}_1 + \vec{e}_2) W_2^-(\vec{n} + \vec{e}_2).$$

Meanwhile, the product for the *reverse* loop is

$$W_2^+(\vec{n}) W_1^+(\vec{n} + \vec{e}_2) W_2^-(\vec{n} + \vec{e}_1 + \vec{e}_2) W_1^-(\vec{n} + \vec{e}_1)$$

so that the ratio of the two probabilities is

$$\left(\frac{M+1}{M} \frac{N-M-1}{N-M-2} \right)^{q_1 - q_2}.$$

Since the quantity in the bracket is strictly greater than unity, this ratio is not unity as long as $q_1 \neq q_2$. Thus, the dynamics of our $2qVZ$ violates the detailed balance. Of course, setting $q_1 = q_2$ we recover the $qVMZ$, for which the above ratio is always unity, confirming that the single- q case of Ref. [16] satisfies the detailed balance.

Violation of detailed balance has a number of consequences on the behavior of a system. These will be scrutinized in the next sections. In particular, we will be mostly interested in the behavior of the stationary state (reached after very long times from any initial \vec{n}_0), described by the T -independent distribution $P^*(\vec{n})$ [25]. From Eq. (1), we see that it is the (right) eigenvector of \mathcal{G} with unit eigenvalue. Meanwhile, the joint distribution in this state will be homogeneous in time and so, depends only on the difference $\tau \equiv T' - T$:

$$\mathcal{P}^*(\vec{n}', T'; \vec{n}, T) = \mathcal{G}^\tau(\vec{n}', \vec{n}) P^*(\vec{n})$$

III. MICROSCOPIC CHARACTERIZATION OF THE NESS

As summarized in Appendix A, a significant consequence of detailed balance violation is that the system relaxes into a *non-equilibrium steady state* (NESS). Typically, finding the associated stationary distribution P^*

is a challenging task [26]. Further, due to the absence of time reversal, this NESS is characterized by non-vanishing probability currents [19]. Though *net* currents may flow between any two configurations in general, here they exist only between nearest neighbors, e.g., from \vec{n} to $\vec{n} + \vec{e}_i$. Thus, we can denote it by a vector field \vec{K}^* , the components being

$$\begin{aligned} K_1^*(\vec{n}) &= W_1^+(\vec{n})P^*(\vec{n}) - W_1^-(\vec{n} + \vec{e}_1)P^*(\vec{n} + \vec{e}_1), \quad (5) \\ K_2^*(\vec{n}) &= W_2^+(\vec{n})P^*(\vec{n}) - W_2^-(\vec{n} + \vec{e}_2)P^*(\vec{n} + \vec{e}_2), \end{aligned}$$

Note that $-K_i^*(\vec{n} - \vec{e}_i)$ is also the net current from \vec{n} to $\vec{n} - \vec{e}_i$. In a NESS, the current is divergence-free (see Appendix A). On a lattice, this condition reads

$$0 = K_1^*(\vec{n}) - K_1^*(\vec{n} - \vec{e}_1) + K_2^*(\vec{n}) - K_2^*(\vec{n} - \vec{e}_2). \quad (6)$$

As a result, the curl of \vec{K}^* is non-trivial, i.e., \vec{K}^* forms closed loops, a useful characterization of which is the vorticity, ω^* (see Appendix A). On the discrete $S_1 \times S_2$ lattice, any closed loop can be regarded as the sum of elementary loops, each around a square (plaquette). Thus, we associate ω^* with a plaquette instead of a site. While the center of a plaquette is located at half integers $(n_1 + 1/2, n_2 + 1/2)$ [27], we will still use \vec{n} for convenience. Thus we write

$$\omega^*(\vec{n}) = K_1^*(\vec{n}) + K_2^*(\vec{n} + \vec{e}_1) - K_1^*(\vec{n} + \vec{e}_2) - K_2^*(\vec{n}). \quad (7)$$

Of course, ω^* is related to the (generalized) discrete Laplacian of P^* and so, carries information about the curvature of P^* . At the intuitive level, such loops also suggest that one species “following”, or “chasing”, the other (see Fig. 3(b,c)), much like the time-irreversible dynamics of predator-prey systems.

Apart from the vorticity, it is useful to characterize a divergence free vector field as the curl of another. Since our space is two dimensional, this field is a scalar, ψ^* , known in fluid dynamics as the stream function. Thus,

$$K_i^*(\vec{n}) = \varepsilon_{ij} [\psi^*(\vec{n}) - \psi^*(\vec{n} - \vec{e}_j)] \quad (8)$$

where ε_{ij} is the two-dimensional Levi-Civita symbol and repeated indices are summed. On our lattice, ψ^* is also associated with a plaquette so that we can use the same scheme as in ω^* . If we chose the arbitrary constant in ψ^* to be zero just outside the $S_1 \times S_2$ rectangle, then we find

$$\psi^*(\vec{n}) = \sum_{\ell=0}^{n_2} K_1^*(n_1, \ell) = - \sum_{\ell=0}^{n_1} K_2^*(\ell, n_2), \quad (9)$$

For the more familiar continuum versions of \vec{K}^* , ω^* , and ψ^* , see Appendix A 1.

Finally, in formal analogy with fluid dynamics, we can associate these probability current loops with the concept of *probability angular momentum*. As $\vec{L} = \int_{\vec{r}} \vec{r} \times \vec{J}(\vec{r})$ represents the total angular momentum of a fluid with current density \vec{J} , the sum $\sum_{\vec{n}} [n_1 K_2^*(\vec{n}) - n_2 K_1^*(\vec{n})]$ plays

the same role in the 2qVZ case. Since $\vec{K}^* \propto P^*$, such a sum can be recognized as a form of statistical average. It is reasonable to label it as the *average* total probability angular momentum (in the NESS):

$$\langle \mathcal{L} \rangle^* \equiv \sum_{\vec{n}} \varepsilon_{ij} n_i K_j^*(\vec{n}). \quad (10)$$

In this context, it is possible to regard \vec{K}^* as a kind of probability distribution, much like P^* . In fact, substituting (5) into this expression leads us to

$$\langle \mathcal{L} \rangle^* = \langle \varepsilon_{ij} n_i V_j \rangle^* \quad (11)$$

where $\vec{V} \equiv \vec{W}^+ - \vec{W}^-$, see Appendix A 1. Clearly, $\langle \mathcal{L} \rangle^*$ is as much as a physical observable in the NESS as the mean $\langle n_i \rangle^* \equiv \sum_{\vec{n}} n_i P^*(\vec{n})$ or the two-point lagged correlations $\langle n_i n_j \rangle_T^* \equiv \sum_{\vec{n}, \vec{n}'} n'_i n_j P^*(\vec{n}', T; \vec{n}, 0)$. Indeed, in the limit of large N , we will see that $\langle \mathcal{L} \rangle^*$ is directly related to the *antisymmetric* part of $\langle n'_i n_j \rangle_{T=1}^*$ [17, 28], see (A9). In subsequent sections, we will devote much of our attention to such quantities.

IV. NUMERICALLY EXACT RESULTS FOR SMALL SYSTEMS

We have already noted that for systems in NESS, it is difficult to find the exact analytic expressions for P^* in general. However, for small systems, it is possible to attain numerically the “exact” P^* numerically to a prescribed accuracy. Once $P^*(\vec{n})$ is known, with (5)-(10), it is then straightforward to compute all other quantities of interest, e.g., the stationary probability current $K^*(\vec{n})$, vorticity $\omega^*(\vec{n})$, stream function $\psi^*(\vec{n})$, angular momentum $\langle \mathcal{L} \rangle^*$, and any correlation function. It should be clear that in this subsection the evolution operator \mathcal{G} is an $(S_1 + 1)(S_2 + 1) \times (S_1 + 1)(S_2 + 1)$ matrix and we consider here the evolution according to (1) in matrix form, i.e. $\vec{P}(T + 1) = \mathcal{G} \vec{P}(T)$, where $\vec{P}(T)$ is the probability vector whose elements are $P(\vec{n}, T)$.

To find a numerically exact $P^*(\vec{n})$ from the evolution operator (2), we thus exploit the matrix relation (1) $\mathcal{G}^\infty \vec{P}(0) = \vec{P}(\infty) = \vec{P}^*$ independently of $\vec{P}(0)$. In practice, we compute $\vec{P}^* = \mathcal{G}^\infty \vec{P}(0)$ by iterating $\mathcal{G}^{2\tau} = \mathcal{G}^\tau \mathcal{G}^\tau$ until the desired accuracy is reached. In particular, for a system with $S_1 = S_2 = 100$, we find P^* accurate up to 10^{-15} with just 64 iterations (i.e. $\mathcal{G}^{2^{64}}$). Since there are $(S_1 + 1) \times (S_2 + 1)$ possible states, the total number of entries in the matrix \mathcal{G} is $[(S_1 + 1)(S_2 + 1)]^2$, which is $O(10^8)$ for $S_1 = S_2 = 100$. Of course, \mathcal{G} is sparse, as there are only five transitions from each state. However subsequent powers of \mathcal{G} soon become dense. This is problematic for calculating the stationary distribution for large systems where one requires a trade off between storing higher powers of \mathcal{G} and the computational cost of repeated multiplications of \vec{P} by \mathcal{G} to some power, in

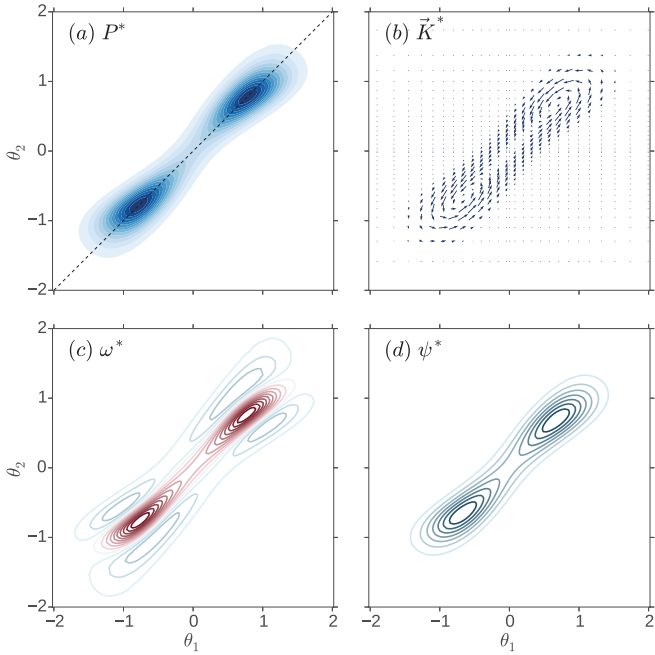


FIG. 3. (Color online). Exact properties of the 2qVZ NESS with $(N, S, Z, q_1, q_2) = (280, 100, 40, 1, 2)$ (low-zealotry phase). (a) Heat maps of the stationary distribution P^* in θ -space where P^* 's peaks are on the dotted line $\theta_1 = \theta_2$, see text. Areas of higher probability appear darker. (b) Stationary probability currents, \vec{K}^* . (c) Stationary vorticity ω^* in θ -space. Regions where ω^* is positive/negative are in red/blue (dark/light in grayscale). (d) Stationary stream function, ψ^* .

order to reach the stationary state quickly. Nevertheless, for systems larger than $S = 100$, it is possible to attain accurate \vec{P}^* 's relatively quickly by exploiting a method which combines iteration and interpolation (see Appendix B).

As briefly explained in Ref. [17], the stationary distribution of the 2qVZ is characterized by two phases in general (as in the qVMZ [16]): When the fraction of zealots is low, the long-time opinion distribution P^* is bimodal (*low-zealotry phase*) whereas it is single-peaked when the density of zealotry exceeds a critical value (*high-zealotry phase*). While this scenario will be scrutinized in the next sections, it is useful to gain some insight by considering some typical systems.

In many ways, the qualitative behavior of the 2qVZ resembles that of the mean-field version of the two-dimensional Ising model. The sum and difference, $(Z_+ + Z_-)/N$ and $(Z_+ - Z_-)/N$, play the role of temperature and external magnetic field, respectively. Thus, the transition in P^* from displaying a single peak to being bimodal as zealotry is lowered. In the latter case, the two peaks are of equal height only when $Z_+ = Z_-$ and the system exhibits *criticality*. Similar to the Ising model in a magnetic field, the 2qVZ is no longer critical when $Z_+ \neq Z_-$ and the bimodal stationary probability is characterized by one peak that vanishes with the system

size. While this phenomenology has also been observed in the qVMZ [16], the 2qVZ is genuinely out-of-equilibrium and it settles into a NESS whose quantitative features are shaped by non-trivial probability currents.

Using the methodology outlined above, we have explored the NESS of systems of various sizes up to $S_1 \times S_2 = 100 \times 100$. For the sake of illustration, we show typical results for P^* , \vec{K}^* , ω^* , and ψ^* in Fig. 3, for the *low zealotry* phase in the symmetric case $S_1 = S_2 = 100$ and $Z_{\pm} = 40$. Of course, the natural variables are just n_i/S_i , the fractions of each population holding opinion +1. On the other hand, there are some advantages to using a different set of variables: $\theta_i = (1/q_i) \ln((S_i/n_i) - 1)$. First, the physical θ 's occupy the entire plane, i.e. $\theta \in (-\infty, \infty)$, while the Ising-like symmetry of the 2qVZ corresponds to $\theta_i \leftrightarrow -\theta_i$. Second, the symmetry point $n_i = S_i/2$, is mapped to the origin. Finally, though there is no symmetry under the exchange of the two populations ($i = 1 \leftrightarrow 2$), we see that $P^*(\vec{\theta})$ is nearly symmetric under this reflection, see Fig. 3(a). In particular, as will be shown below, the fixed points of the deterministic mean-field rate equations (15), which correspond to the peaks of P^* , are situated on the $\theta_1 = \theta_2$ line. Indeed, the “ridge” which runs from one peak through the saddle to the other is seen to lie very close to this line. In Fig. 3(b), we show the current field \vec{K}^* , which whirls around each peak of P^* . These whirls imply correlations of the dynamic properties of the two populations, indicating the tendency of q_2 -voters to “follow” or “chase” q_1 -voters [17], a result that is corroborated by two-point correlation functions in Sec. IV.B. The bottom panels of Fig. 3 show the associated vorticity field and stream function. As expected, ω^* is positive near the peaks, corresponding to the current whirling counter-clockwise. Counter rotations ($\omega^* < 0$) are present away from the peaks, a property not readily discerned when we examine the currents in Fig. 3(b). Lastly, we observe that the stream function ψ^* appears to be very similar to P^* . This behavior is not a coincidence, as we will show that, in the linear Gaussian approximation, the two are strictly proportional to each other.

V. CONTINUUM DESCRIPTIONS AND SIMULATION STUDIES OF LARGE SYSTEMS

As is often the case, the exact description of the 2qVZ through the master equation is intractable and difficult to analyze when the system size is large. Typically, Monte Carlo simulations are needed to explore their behavior. However, much insight can be gained through a continuum description and judicious approximations. Specifically, we consider the thermodynamic limit: $Z_{\pm}, S_i, N \rightarrow \infty$, with fixed densities $z_{\pm} = Z_{\pm}/N$ and $s_i = S_i/N$. In this limit, we expect demographic fluctuations to be negligible and the description in terms of mean-field rate equations is suitable. For large but finite systems, we can account for fluctuations and cor-

relations via the Fokker-Planck equation (FPE) [29] associated with Eq. (1).

A. The Fokker-Planck Equation

When $N \gg 1$, the configuration space of densities $x_i = n_i/N$ approaches the continuum within a rectangle: $x_i \in [0, s_i]$, while time is rescaled so that $t = T/N$ is continuous. In other words, we will say that one Monte Carlo step (1 MCS) corresponds to N moves of the microscopic model. Following standard procedures [21] to obtain the continuum limit of the ME (1), we arrive at the FPE for the probability density $P(\vec{x}; t)$:

$$\frac{\partial}{\partial t} P(\vec{x}; t) = \sum_{i=1,2} \frac{\partial}{\partial x_i} \left[\frac{\partial}{\partial x_i} u_i(\vec{x}) P(\vec{x}; t) - v_i(\vec{x}) P(\vec{x}; t) \right] \quad (12)$$

where $u_i \equiv (w_i^+ + w_i^-)/2N$ and $v_i \equiv w_i^+ - w_i^-$, and where $w_i^+ = (s_i - x_i)(z_+ + x_1 + x_2)^{q_i}$ and $w_i^- = x_i(z_+ + x_1 + x_2)^{q_i}$ are the continuum counterparts of W_i^\pm . The right-hand-side (RHS) can be identified as the divergence of the *probability current density*

$$K_i(\vec{x}; t) = v_i P(\vec{x}; t) - \partial_i [u_i P(\vec{x}; t)] \quad (13)$$

where $\partial_i \equiv \partial/\partial x_i$. Clearly, in the NESS $P(\vec{x}; t) \rightarrow P^*(\vec{x})$, whereas the corresponding stationary probability current density is $K_i^*(\vec{x}) = v_i P^*(\vec{x}) - \partial_i [u_i P^*(\vec{x})]$. To find P^* , we must solve the partial differential equation $\sum_{i=1,2} \partial_i [\partial_i u_i(\vec{x}) P^*(\vec{x}) - v_i(\vec{x}) P^*(\vec{x})] = 0$ with non-trivial boundary conditions: vanishing of the normal components of \vec{K}^* . Thus, obtaining P^* analytically in general is still quite challenging.

B. Mean-Field Analysis

A standard alternative to studying the FPE for the full distribution is to consider the equations governing the evolution of averages of various quantities [30]. In particular, it is intuitively interesting to study the behavior of the average $\langle x_i \rangle_t \equiv \int x_i P(\vec{x}, t) d\vec{x}$. Its evolution is governed by

$$\frac{d}{dt} \langle x_i \rangle = \int x_i \frac{\partial}{\partial t} P(\vec{x}, t) d\vec{x} = \int K_i(\vec{x}) d\vec{x}$$

since the surface contributions from the integration by parts involve the normal components of \vec{K} and vanish. To make progress, we will need to make approximations. First, $\int \partial_i [u_i P]$ is also a surface term. Though it is not necessarily zero, it vanishes at the lowest order for large N . In this limit, we are left with contributions arising only from the first term on the right-hand-side of (13):

$$\begin{aligned} \frac{d}{dt} \langle x_i \rangle &= \langle v_i(\vec{x}) \rangle \\ &= \langle (s_i - x_i)(z_+ + x_1 + x_2)^{q_i} \rangle - \langle x_i(z_+ + x_1 + x_2)^{q_i} \rangle. \end{aligned} \quad (14)$$

Second, we invoke the mean-field approximation (MFA), which assumes that higher moments can be factored in terms of the averages $\langle x_i \rangle$ (e.g., $\langle x_i x_j \rangle \approx \langle x_i \rangle \langle x_j \rangle$). In this sense, the MFA neglects all correlations and fluctuations, an approach that becomes exact when $N \rightarrow \infty$. Within this approach, Eq. (14) becomes the mean-field rate equations (REs) [31] :

$$\frac{d}{dt} x_i = (s_i - x_i) \mu^{q_i} - x_i (1 - \mu)^{q_i} \quad (15)$$

where $\mu = z_+ + x_1 + x_2$ is the density of voters holding opinion +.

The fixed points (FP) of these rate equations are stable or unstable nodes (no limit cycles in our case [17, 27]). They are given by

$$x_i^* = \frac{s_i}{1 + \rho^{q_i}}, \quad (16)$$

where $\rho = (1 - \mu^*)/\mu^*$, with $\mu^* = z_+ + x_1^* + x_2^*$. Note that ρ is the ratio, in the steady state, of voters holding opinion – to those with the + opinion. It satisfies

$$\frac{1}{1 + \rho} = z_+ + \sum_{i=1,2} \frac{s_i}{1 + \rho^{q_i}}. \quad (17)$$

since the left hand side is $\mu^* = z_+ + x_1^* + x_2^*$, which equals the right hand side. In terms of the variables θ_i introduced above, we recognize that $x_i = s_i / (1 + e^{q_i \theta_i})$, so that all FPs are given by $\theta_i^* = \ln \rho$.

We are particularly interested in the case $z_+ = z_- = z$ for which the 2qVZ exhibits a continuous phase transition. In this case, it is clear that $\rho = 1$ ($\mu^* = 1/2$) is always a solution to Eq. (17), corresponding to the “central FP”: $\vec{x}^* = \vec{x}^{(0)} \equiv (s_1/2, s_2/2)$. The properties of this FP changes, as z is decreased below a critical value z_c , from being stable to unstable. To show this property, we linearize Eq. (15) about a FP \vec{x}^* and find the linear stability matrix, $-(\partial x_i / \partial x_j)|_{\vec{x}=\vec{x}^*}$, to have the form

$$\mathbb{F}(\vec{x}^*) = \begin{pmatrix} Y_{1\mu} - X_{1\mu} & -X_{1\mu} \\ -X_{2\mu} & Y_{2\mu} - X_{2\mu} \end{pmatrix}, \quad (18)$$

where

$$\begin{aligned} Y_{i\mu} &= \mu^{q_i} (1 + \rho^{q_i}), \\ X_{i\mu} &= q_i x_i^* (1 - \mu^*)^{q_i-1} (1 + \rho). \end{aligned}$$

Evaluating $\det \mathbb{F}$ at $\vec{x}^* = \vec{x}^{(0)}$, we find a remarkably simple result:

$$\det \mathbb{F}(\vec{x}^{(0)}) = 2^{2-q_1-q_2} [1 - q_2 s_2 - q_1 s_1] \quad (19)$$

Since a stable FP is associated with $\det \mathbb{F}(\vec{x}^{(0)}) > 0$, this expression implies that the 2qVZ resembles an Ising model at high temperatures when

$$1 > s_1 q_1 + s_2 q_2. \quad (20)$$

In the case $\det \mathbb{F}(\vec{x}^{(0)}) < 0$, $\vec{x}^{(0)}$ turns unstable and we can verify that there are two other (real ρ) solutions

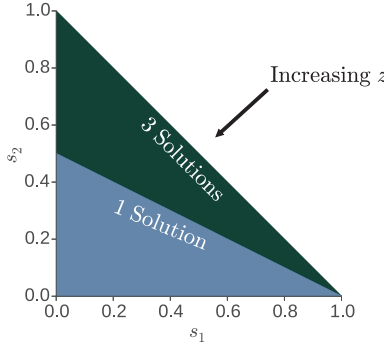


FIG. 4. (Color online). Criticality in the $2qVZ$ ($z_{\pm} = z$): Dependence of z_c on the susceptible densities. Criticality at z_c occurs on the interface between the blue/grey and green/black regions, prescribed by $s_1q_1 + s_2q_2 = 1$, and the corresponding critical zealotry density is $z_c = (1 - s_1 - s_2)/2$, see text. In the blue/grey region, the mean-field equations (15) have one fixed point, whereas they admit three fixed points in the green/black region, see text. Here, $(q_1, q_2) = (1, 2)$.

to Eq. (17), corresponding to two other stable, “non-central” FPs: $\vec{x}^{(\pm)}$. Of course, these correspond to the low temperature phase of the Ising model, with a spontaneously broken symmetry. Thus, we will refer to the line $s_1q_1 + s_2q_2 = 1$ as the critical line (plotted in Fig. 4), separating the s_1 - s_2 plane into a region where $\vec{x}^{(0)}$ is the sole FP and another where Eq. (15) admits three FPs. Before continuing, we emphasize that this technique is powerful enough for us to obtain the generalization of (20) to a population with any number of groups of q_i -voters, namely, $\vec{x}^{(0)}$ is stable when $1 > \sum_i s_i q_i$. Details are given in Appendix C.

Since $1 = 2z + s_1 + s_2$, we can express the critical z_c as a function of the q ’s and the difference $\Delta s \equiv s_1 - s_2$

$$z_c = \frac{\bar{q} - 1}{2\bar{q}} + \frac{q_1 - q_2}{q_1 + q_2} \frac{\Delta s}{2}, \quad (21)$$

where \bar{q} is the average $(q_1 + q_2)/2$. In the limit of a homogeneous population ($q_1 = q_2$), we recover the critical values $z_c = (q - 1)/(2q)$ of the q VMZ [16]. In this spirit, we may introduce an *effective* q_{eff} for our heterogeneous $2qVZ$:

$$q_{\text{eff}} = \frac{s_1q_1 + s_2q_2}{s_1 + s_2} \quad (22)$$

in the sense that the number of FPs in the $2qVZ$ are the same as those in the homogeneous q VMZ with this q_{eff} . Indeed, as shown in Appendix C, this notion can be generalized to $q_{\text{eff}} = (\sum_i s_i q_i) / (\sum_i s_i)$ in the case of populations with any composition.

C. Beyond MFA for Systems Far from Criticality

While the MFA provides an adequate picture of the deterministic aspects of the system’s evolution and the location of a phase transition, it cannot capture the stochastic

nature of our model. In this section, we study the influence of demographic fluctuations in finite populations by means of the linear Gaussian approximation (LGA) of the FPE (12) [17, 19]. To be concise, we focus on systems with symmetric zealotry ($z_{\pm} = z$) far from criticality, i.e., $z \ll z_c$ and $z \gg z_c$. In the realm of the LGA, we are able to compute many quantities of interest exactly, in the NESS. Beyond the LGA, we also study the mean switching time that characterizes the stochastic dynamics in the low zealotry phase when the system endlessly switches between the two stable fixed points $\vec{x}^{(\pm)}$.

1. Linear Gaussian Approximation of P^*

To describe fluctuations in the NESS, we examine the FPE (12) beyond the lowest order in $1/N$. This procedure can provide a scaling analysis of typical non-critical fluctuations in systems of large but finite size N . As our focus is the behavior in a NESS, we consider small deviations near a (stable) fixed point \vec{x}^* : $\vec{\xi} = \vec{x} - \vec{x}^*$. The LGA consists of linearizing the drift term of (12), i.e. $v_i \rightarrow (-\mathbb{F} \cdot \vec{\xi})_i$, while the diffusion coefficient is evaluated at $\vec{x}^* = (x_1^*, x_2^*)$, i.e. $u_i \rightarrow w_i^* = w_i^+(\vec{x}^*) = w_i^-(\vec{x}^*)$. Upon substitution into FPE (12), we obtain the LGA-FPE for the stationary distribution:

$$0 = \sum_{i=1,2} \frac{\partial}{\partial \xi_i} \left[\frac{\partial}{\partial \xi_i} D_{ij} + \sum_{j=1,2} F_{ij} \xi_j \right] P^*(\vec{\xi}). \quad (23)$$

Here, D_{ij} and F_{ij} are the elements of the diffusion matrix $\mathbb{D}(\vec{x}^*)$ and the drift matrix $\mathbb{F}(\vec{x}^*)$, respectively. The former is given by

$$\mathbb{D}(\vec{x}^*) = \frac{1}{N} \begin{pmatrix} x_1^*(1 - \mu^*)^{q_1} & 0 \\ 0 & x_2^*(1 - \mu^*)^{q_2} \end{pmatrix} \quad (24)$$

(i.e., $D_{ij} = \delta_{ij} w_i^*/N$), while \mathbb{F} is given by (18) [32]. In general, the solution of (23) is still a Gaussian [21]:

$$P^*(\vec{\xi}) \propto \exp \left[-\frac{1}{2} \vec{\xi} \cdot \mathbb{C}^{-1} \vec{\xi} \right], \quad (25)$$

where \mathbb{C} is the covariance matrix, with elements

$$C_{ij} = \langle \xi_i \xi_j \rangle^*, \quad (26)$$

and can be obtained from \mathbb{D} (24) and \mathbb{F} (18) by solving $\mathbb{F}\mathbb{C} + \mathbb{C}\mathbb{F}^T = 2\mathbb{D}$ [22]. Details, as well as the explicit forms for \mathbb{C} in our case can be found in Appendix D. Since \mathbb{D} is $O(1/N)$ and \mathbb{F} is $O(1)$, it follows that \mathbb{C} is also $O(1/N)$, confirming our expectation that the fluctuations (standard deviations) are $O(1/\sqrt{N})$. Needless to say, if we approach criticality, then one of the eigenvalues of \mathbb{F} approaches zero, so that \mathbb{C} diverges and this approximation breaks down. On the other hand, for fixed $z \neq z_c$, the accuracy of the Gaussian expression (25) improves as $N \rightarrow \infty$. As an example of the quality of the

LGA, we find that, for $N = 400$ and $S_i = Z_{\pm} = 100$, the prediction from (25) with (D2) agrees with the numerically exact P^* to $\lesssim 2\%$ within about two standard deviations.

2. Currents and correlations in the LGA[33]

With a known P^* , we can find two exact expressions for the currents $\vec{K}^* = -\{\mathbb{D}\vec{\nabla} + \mathbb{F}\vec{\xi}\} P^*$. One displays the linear relationship $\vec{K}^* \propto \vec{\xi}P^*$:

$$\vec{K}^*(\vec{\xi}) = \{\mathbb{D}\mathbb{C}^{-1} - \mathbb{F}\} \vec{\xi}P^*(\vec{\xi}). \quad (27)$$

The other shows explicitly that \vec{K}^* is divergence free:

$$\vec{K}^*(\vec{\xi}) = \frac{\mathbb{F}\mathbb{C} - \mathbb{C}\mathbb{F}^T}{2} \vec{\nabla}P^*(\vec{\xi}),$$

where we have used $\mathbb{D} = [\mathbb{F}\mathbb{C} + \mathbb{C}\mathbb{F}^T]/2$. The key observation here is that the matrix is antisymmetric, which leads us to define

$$\mathbb{L} = \begin{pmatrix} 0 & L_{12} \\ -L_{12} & 0 \end{pmatrix} \equiv \mathbb{F}\mathbb{C} - \mathbb{C}\mathbb{F}^T \quad (28)$$

In other words, $K_i^* = \varepsilon_{ij}\partial_j(L_{12}P^*/2)$, allowing us to identify the stream function $\psi^* = L_{12}P^*/2$, a linear relationship pointed out above. Further, from the continuum version of (10), we see that [34]

$$\langle \mathcal{L} \rangle^* = \int \varepsilon_{ij}\xi_i K_j^* d\vec{\xi} = L_{12} \quad (29)$$

Meanwhile, the vorticity field is proportional to $\xi_i \xi_j P^*$, so that it can be both positive and negative, as illustrated in Fig. 3(c).

Finally, we turn our attention to the continuum version of the general two point correlation, namely, $\langle \xi_i \xi_j \rangle_{\tau}^* = \int \xi_i' \xi_j P^*(\vec{\xi}', t + \tau; \vec{\xi}, t) d\vec{\xi}' d\vec{\xi}$. In the LGA, it is much easier to use the solution to the Langevin equation: $\vec{\xi}(\tau) = e^{-\mathbb{F}\tau} \vec{\xi}(0)$ plus noise. Since the noise is uncorrelated in time,

$$\langle \xi_i(0) \xi_j(\tau) \rangle^* = e^{-F_{jk}\tau} \langle \xi_i(0) \xi_k(0) \rangle^* = C_{ik} e^{-F_{ik}\tau}$$

The antisymmetric part of this correlation is necessarily odd in τ and does not vanish for systems in NESS. Also central to our study of NESS, we define the t -independent quantity [17, 20, 28]

$$\tilde{C}(\tau) \equiv \langle \xi_1(t) \xi_2(t + \tau) \rangle^* - \langle \xi_2(t) \xi_1(t + \tau) \rangle^* \quad (30)$$

which is the 12 element of the matrix

$$\tilde{\mathbb{C}}(\tau) = \mathbb{C} e^{-\mathbb{F}^T \tau} - e^{-\mathbb{F} \tau} \mathbb{C} \quad (31)$$

Since $v_i(0) = d\xi_i/d\tau|_{\tau=0}$, we see that the continuum version of (11) is $\langle \mathcal{L} \rangle^* = \langle \varepsilon_{ij} \xi_i v_j \rangle^*$, which implies

$$\frac{d\tilde{C}}{d\tau} \bigg|_{\tau=0} = \langle \mathcal{L} \rangle^*; \quad \frac{d\tilde{\mathbb{C}}}{d\tau} \bigg|_{\tau=0} = \mathbb{F}\mathbb{C} - \mathbb{C}\mathbb{F}^T \quad (32)$$

within the LGA. Thus, we can regard $\tilde{C}(\tau)$ as a generalized probability angular momentum, further details of which will be provided in the next subsection.

3. Simulation results for the symmetric case

$$s_{1,2} = s, z_{\pm} = 1/2 - s$$

The above expressions (25)-(31) carry significant information on the NESS of the $2qVZ$ in the realm of the LGA and are valid for any values of $s_{1,2}$ and $q_{1,2}$. Here, we report the explicit results obtained for the symmetric case $s_{1,2} = s, z_{\pm} = \frac{1}{2} - s$ ($q_2 = 2q_1 = 2$). These results complete those in Ref. [17] and allow us to discuss the validity of the LGA by considering a concrete example. Here, the explicit expressions of C_{ij} , the stationary correlation functions $\langle \xi_i \xi_j \rangle^*$, are given by (D2) and (D4), while the corresponding drift matrices \mathbb{F} have been given in Ref. [27] along with their (real and distinct) eigenvalues labelled by λ_{\pm} , where $\lambda_+ > \lambda_-$.

To assess the validity of the LGA, we have performed Monte Carlo simulations of large systems with N up to 14,400, and compiled histograms from the trajectories to find the probability distribution $P^*(\vec{n})$. Similar to the comparison with the LGA prediction for smaller systems above, we find that (25) is an excellent approximation in the high-zealotry phase, i.e. $P^*(\vec{\xi}) \simeq NP^*(\vec{n})$, with a sharp peak around the symmetric FP $\vec{x}^{(0)}$. In the low zealotry phase, we have confirmed that the stationary probability density is bimodal, with two sharp peaks close to the mean-field FPs $\vec{x}^{(\pm)}$. However, the distribution around each FP [35] is both skewed and more sharply peaked than the LGA prediction. For systems with $N \lesssim 10^3$ visible deviations between (25) and simulation results exist. Yet, for larger systems ($N \gg 10^3$), the agreements are quite reasonable, even in the low zealotry phase. We have confirmed this analysis by computing the skewness and (excess) kurtosis of in the 1D projections [36] of $P^*(\vec{\xi})$ onto each axis in both regimes. For the smallest system we considered ($S = 250$), in the low zealotry regime $Z = 100$ the kurtosis was $(-0.242, 0.750)$ for the ξ_1 and ξ_2 projections respectively. The skewness was $(0.321, 0.969)$. For the high zealotry regime $Z = 200$ the kurtosis was $(-0.030, -0.130)$ and skewness $(0.004, -0.007)$, confirming that the LGA is a better approximation at the high zealotry regime.

As the system size increases the kurtosis and skewness approach zero for both regimes. In Fig. 5, the LGA predictions (D2) and (D4) in the high/low zealotry phases are compared against the simulation results for $\langle \xi_i \xi_j \rangle^*$. The outcome confirms that $C_{ij} \propto 1/N$, i.e. fluctuations scale as $N^{-1/2}$, in both phases far from criticality. However, while the LGA provides a good quantitative predictions for $N \gtrsim 10^3$ in the $z > z_c$ cases, much larger system sizes ($N \gg 10^3$) are necessary to reach a similar quantitative agreement in the low-zealotry phase. We believe that the significant skewness associated with $\vec{x}^{(\pm)}$ in the latter regime when N is not sufficiently large is respon-

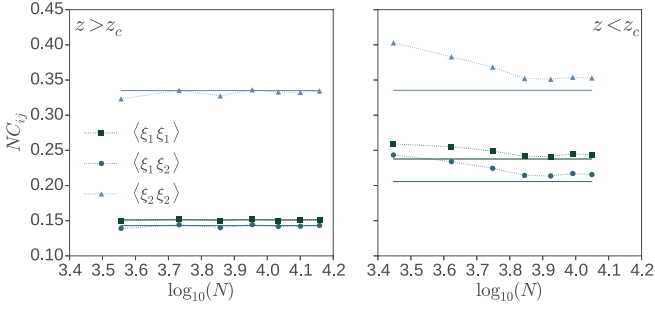


FIG. 5. (Color online). $C_{ij} = \langle \xi_i \xi_j \rangle$ a function of system size N : Comparison of the LGA predictions (D2) (left panel) and (D4) (right panel) in dashed against results of stochastic simulations (solid), averaged over at least 10^5 MCS. The scaling $C_{ij} \propto 1/N$ is confirmed and the quantitative agreement improves as N increases (with reasonably good agreement in the low-zealotry phase when $N \gg 10^3$). Here, $s_{1,2} = s$, $z_{\pm} = z = \frac{1}{2} - s$ with $q_2 = 2q_1 = 2$. In the two regimes $z > z_c$ and $z < z_c$ we have $z = 2/9$ and $z = 1/7$ respectively, the critical value being $z_c = 1/6$.

sible for the differences. A better and systematic understanding of this phenomenon is desirable, but beyond the scope of this study. Using Eq. (5), we can compute the probability current \vec{K}^* exactly (for small systems) or via simulations and compare the results with the current obtained from Eq. (27) by using P^* obtained within the realm LGA as shown in Fig. 6. From this comparison, we notice that due to finite size effects the MF fixed point and peaks of the distribution (around which \vec{K}^* whirls) do not coincide perfectly, and the LGA flows are not symmetric around the fixed point. These discrepancies between simulations of the original 2qVZ and the LGA predictions are attenuated and eventually dissipate when the system size is increased. Furthermore, we also verified that, as predicted by the LGA, the stream function is always positive, in agreement with the counter-clockwise whirls of the probability current near the peaks reported in Fig. 3(b,c) and Fig. 6.

Turning to the antisymmetric two-point correlation function in the NESS $\tilde{C}(\tau)$, we find $\tilde{C}(\tau)$ from the simulation trajectories $\vec{x}_i(t)$ via the lagged correlation: $\frac{1}{R-\tau} \sum_{t=0}^{R-\tau} [x_1(t)x_2(t+\tau) - x_2(t)x_1(t+\tau)]$, where R is the length of our run (typically, 10^5 MCS). From Eq. (31) we have

$$\tilde{C}(\tau) = \langle \mathcal{L} \rangle^* \left(\frac{e^{-\lambda_- \tau} - e^{-\lambda_+ \tau}}{\lambda_+ - \lambda_-} \right)$$

where λ_{\pm} are the eigenvalues of \mathbb{F} . In Fig. 7 we plot the LGA expression of \tilde{C} and the same quantity obtained from stochastic simulations and again find a good agreement in both high- and low-zealotry regimes. In particular, we notice that the LGA accurately captures the peak of $\tilde{C}(\tau)$ at $\tau^* = [\ln(\lambda_+/\lambda_-)]/[\lambda_+ - \lambda_-]$ [17]. As illustrated in Fig. 7, the 2qVZ is characterized by $\tilde{C}(\tau) > 0$, i.e. q_1 -susceptibles are correlated in such a

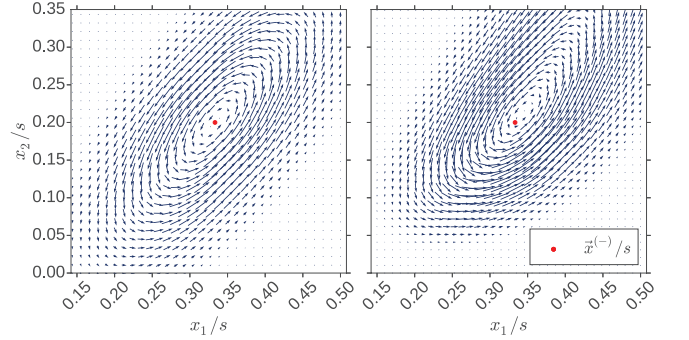


FIG. 6. (Color online). Stationary probability current: Comparison of the LGA predictions Eq. (27) (left panel) with the numerically exact counterpart Eq. (5) (right panel) near the fixed point $x^{(-)}$ (red/grey dot) in the low zealotry phase, see text. Parameters here are $(N, S_1, S_2, Z, q_1, q_2) = (280, 100, 100, 40, 1, 2)$.

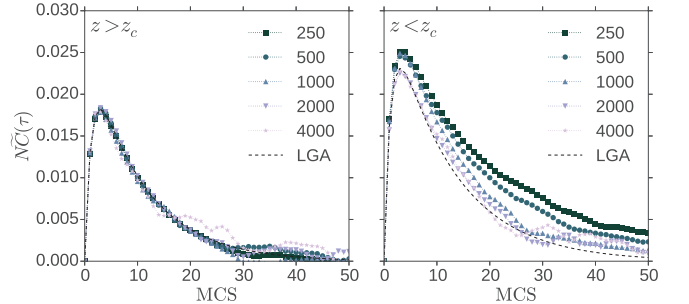


FIG. 7. (Color online). LGA prediction of the two point correlation function, $\tilde{C}(\tau)$ (dashed) compared to simulations (solid) in the high (left) and low (right) zealotry regimes for the symmetric case $s_{1,2} = s$, $z_{\pm} = z = \frac{1}{2} - s$ with $q_1 = 1$ and $q_2 = 2$. In the high zealotry regime, the LGA captures the behavior of \tilde{C} for all values of S considered. For the low zealotry regime the LGA is qualitatively accurate for all S , however only qualitatively accurate for $S \geq 2000$. Fluctuations for MCS greater than 20 are due to a low sampling rate. The LGA values for the peak τ^* for the high and low zealotry regimes, 2.80 and 3.05 respectively, accurately predict the data peak which occurs at 3 in both cases.

way that $\langle x_1(t)x_2(t+\tau) \rangle^* > \langle x_2(t)x_1(t+\tau) \rangle^*$. This indicates that on a finite timescale (up to a separating time $\tau \approx 40 - 50$ in Fig. 7) q_2 -voters are more likely to “follow” q_1 -susceptibles than vice-versa. Clearly, for large lag times ($\tau \gg \lambda_{\pm}$), $\tilde{C} \rightarrow 0$ and correlations are lost.

D. Fluctuation Driven Dynamics below Criticality - Switching Times

Similarly to what happens in the q VMZ [16] (see also [37]), the long-time behavior in the low zealotry phase is characterized by a “swing-state dynamics”, or “switching dynamics” when there is the same number of zealots of both types or when there is only a small

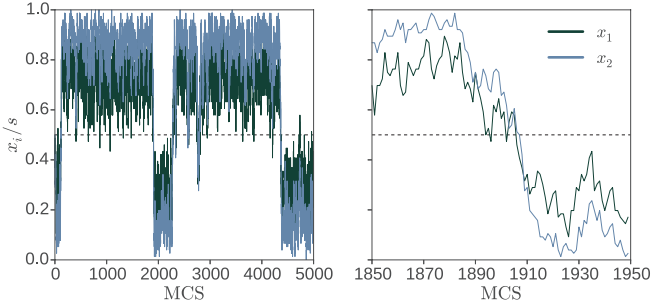


FIG. 8. (Color online). Switching behaviour of the 2qVZ at $z < z_c$: Time series for the total density of +1 susceptible voters within each population (x_i/s_i). Sample of 5000 MCS (left) and closer examination of a typical switching period (right). One unit of time $t = \tau/N$ is 1 MCS and equates to N iterations of the model. Here parameters are: $(N, s_1, s_2, z, q_1, q_2) = (200, 0.38, 0.38, 0.12, 1, 2)$.

asymmetry in the zealotry. In the switching dynamics both the q_1 - and q_2 -susceptibles suddenly switch ‘almost’ simultaneously between the peaks $x_i^{(\pm)} \approx 0, s$ of $P^*(\vec{x})$, see Fig. 8. As explained above, q_2 -voters “follow” q_1 -voters and therefore q_1 -susceptibles switch before q_2 -susceptibles, however the lag between the switching of both populations is negligible in a first approximation, as shown in Fig. 8 (right), and will be neglected in what follows. In the remainder of this subsection, we focus on the case of symmetric zealotry, $z_{\pm} = z$.

This switching phenomenon that is driven by fluctuations, and therefore is beyond the reach of the mean-field analysis, can be analyzed in terms of the *mean switching time* τ_s , measures the mean time to switch from one peak of $P^*(\vec{x})$, say $(x_1^{(-)}, x_2^{(-)})$, to the other, $(x_1^{(+)}, x_2^{(+)})$ for the first time [16].

Finding the mean switching time can be formulated as a first-passage problem whose solution, in terms of the FPE or the Kramer’s escape theory [38], is simple only in the single-variate case of a single type of susceptibles as in the *qVMZ* [16]. However, as here the 2qVZ violates the detailed balance, the problem is much more complicated.

An approximation of τ_s is obtained by exploiting the mapping onto the *qVMZ* for values of z just below the critical value z_c ($z \lesssim z_c$). In this regime, we expect that the switching dynamics of the 2qVZ with (q_1, q_2) can be approximately mapped onto that of the *qVMZ* with an effective value q_{eff} given by (22). In this approximation the mean switching time between the two fixed points can be computed as in Ref. [16] by solving $\mathcal{G}_b^{\text{eff}}(x_1)\tau_s(x_1) = -1$ with the reflective and absorbing conditions $(d/dx_1)\tau_s(x_1^{(-)}) = \tau_s(x_1^{(+)}) = 0$, which yields

$$\tau_s = 2N \int_{x_1^{(-)}}^{x_1^{(+)}} dy e^{-N\phi(y)} \int_{x_1^{(-)}}^y \frac{e^{N\phi(v)} dv}{\tilde{w}^+(v) + \tilde{w}^-(v)}, \quad (33)$$

where $\phi(v) = 2 \int_{x_1^{(-)}}^v \left\{ \frac{\tilde{w}^+(v) - \tilde{w}^-(v)}{\tilde{w}^+(v) + \tilde{w}^-(v)} \right\}$. Now, $\tilde{w}^+(x) = (s_1 + s_2 - x)(x + z)^{q_{\text{eff}}}$ and $\tilde{w}^-(x) = x(s_1 + s_2 + z - x)^{q_{\text{eff}}}$

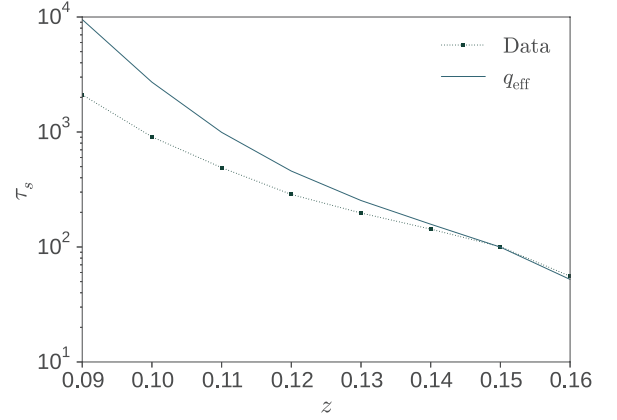


FIG. 9. (Color online). Mean switching time τ_s between the two stable fixed points for systems of size $N = 100$ with $(q_1, q_2) = (1, 2)$. Results obtained from stochastic simulations (blue \square) are compared with the approximations (33) (blue/dark gray) and (34) (green/light gray), see text. Simulation data are averaged over 10^6 MCS. Here $s_{1,2} = s = \frac{1}{2} - z$.

and therefore, using the Kramers’ formula [16, 38], we have

$$\ln \tau_s \simeq 2N \int_{x_1^{(-)}}^{x_1^{(+)}} \frac{\tilde{w}^-(y) - \tilde{w}^+(y)}{\tilde{w}^-(x^{(-)}) + \tilde{w}^+(x^{(-)})} dy \quad (34)$$

which predicts that the mean switching time τ_s grows (approximately) exponentially with N [16]. The results reported in Fig. 9 confirm that this approximation is accurate just below z_c , while it overestimates τ_s at lower values of z . The fact that the mean switching time in the 2qVZ is generally shorter than in its equilibrium *qVMZ* (with $q = q_{\text{eff}}$) counterpart suggests that the probability currents, absent in the *qVMZ*, are responsible for speeding up the switching dynamics by reducing the switching time.

E. Behavior Near Criticality

Up to now, we have mostly focused on the properties on the 2qVZ deep in the high-zealotry and low-zealotry phases. Here we focus on some properties of the system close to criticality: $z_{\pm} = z \approx z_c$.

Since, every individual in our system is connected to every other (i.e., a complete graph), we anticipate that a Landau-like description should be adequate to capture the critical behavior. Specifically, we are concerned with how the fluctuations (co-variances C_{ij}) scale with N at criticality. By formal analogy with the standard approach for an Ising magnet, we consider a free energy functional (at zero external magnetic field) [39].

$$\mathcal{F}(m) = N \left\{ \frac{rm^2}{2} + \frac{gm^4}{4} \right\}$$

where r is a measure of the deviation from the critical point (e.g., $T - T_c$) and $g > 0$. Thus, using

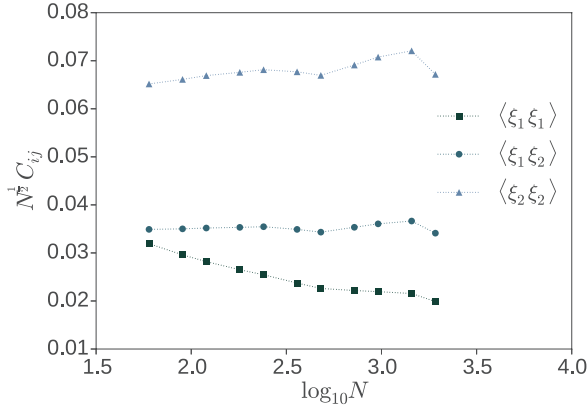


FIG. 10. (Color online). Correlations as a function of system size $\log_{10}(N)$ for simulated results, averaged over at least 10^5 MCS. The fluctuations roughly scale as $N^{-1/2}$ as predicted. Here the parameters are: $(s_1, s_2, z, q_1, q_2) = (\frac{1}{3}, \frac{1}{3}, \frac{1}{6}, 1, 2)$. N varies from $N = 60$ to 1920.

$P(m) \propto e^{-\mathcal{F}}$, we find $\langle m^2 \rangle \propto N^{-1}$ and N^0 , above and below criticality respectively - as reported in the previous section. For $r = 0$, however, $\langle m^2 \rangle \propto N^{-1/2}$. In Fig. 10, we report that in line with the above general considerations all three stationary two-point correlation functions $\langle \xi_i \xi_j \rangle$ of the 2qVZ measured from simulations with $z = z_c$ indeed approach this behavior as N increases: $\langle \xi_i \xi_j \rangle \sim N^{-1/2}$.

A full finite-size-scaling analysis of the entire critical region should include (i) the behavior of z_c as a function of N , (ii) the effects of $z_+ \neq z_-$, (iii) the Binder cumulant (excess kurtosis), etc. We fully expect universal behavior, i.e., properties which do not depend on the detailed partition into the two populations (s_1, s_2) . While valuable, such a study is beyond the scope of this paper.

VI. THE 2qVZ WITH ASYMMETRIC ZEALOTRY

In this section we briefly outline the main properties of the 2qVZ with asymmetric zealotry by assuming that, say, $Z_+ > Z_-$.

The 2qVZ with asymmetric zealotry shares qualitatively the same features as its qVMZ counterpart [16]: It also displays a high- and low-zealotry phase which are respectively characterized by a unimodal and bimodal stationary probability distribution P^* . However, the latter are now no longer symmetric: in the low-zealotry phase the peak associated with the opinion supported by Z_+ zealots is much more pronounced than that associated with Z_- zealots (see Fig. 11(left)), whereas the single-peaked distribution in the high-zealotry phase is skewed towards states with a majority of +1 voters. When N is sufficiently large, the peaks of P^* of course correspond to the fixed points of the mean-field equation (15) whose analysis reveals that, as for the qVMZ, in the low-zealotry

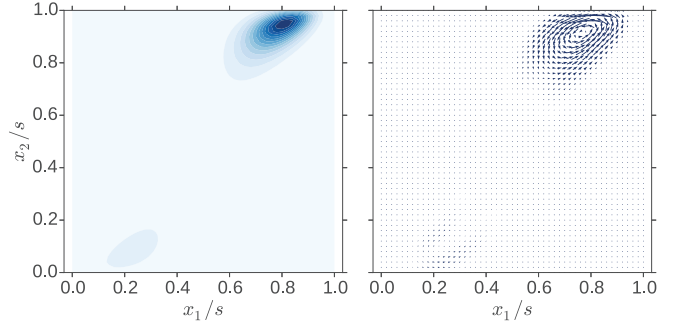


FIG. 11. (Color online). Numerically exact NESS probability distribution P^* and current probability \vec{K}^* in the low-zealotry phase with asymmetric zealotry: (Left) Darkness indicate regions in the $x_1/s - x_2/s$ where P^* is high (P^* being higher where it is darker). (Right) Vector field of the current probability \vec{K}^* . Parameters are: $(N, S_1, S_2, Z_+, Z_-, q_1, q_2) = (258, 100, 100, 30, 28, 1, 2)$.

phase the two stable fixed points $\vec{x}^{(\pm)}$ are separated by the unstable steady state $\vec{x}^{(0)}$, while in the high-zealotry phase only $\vec{x}^{(+)}$ is stable. However, again, a major difference between the 2qVZ and the qVMZ is that the former violates the detailed balance which results in the steady state being a NESS and in a number of intriguing results such as the existence of stationary current of probability that form closed loops in the configuration space. A typical example of the exact NESS probability distribution P^* in the low zealotry phase with $Z_+ > Z_-$ is shown in Fig. 11 along with the wind field of the stationary current probability \vec{K}^* . In Fig. 11(left), we see that even when there is a small asymmetry in the zealotry the peak corresponding to $\vec{x}^{(-)}$ is almost invisible and the distribution is dominated by the peak associated with $\vec{x}^{(+)}$ and whose intensity increases with N . As a consequence, the stationary current probability \vec{K}^* flows mostly around $\vec{x}^{(+)}$ in a anti-clockwise fashion (vorticity is positive), even though there is current flow around $\vec{x}^{(-)}$ but with a much smaller amplitude. These features of the 2qVZ with asymmetric zealotry can be analyzed using the techniques of Sec. IV and more specifically the Fokker-Planck and linear Gaussian approximations in the continuum limit when $N \gg 1$. In fact, we can still use (25)-(31) within the LGA and obtain the stationary probability density $P^*(\vec{\xi})$ near the fixed points in each of the phase, as well as the LGA expressions of the stationary density current $\vec{K}^*(\vec{\xi})$, correlation functions $C_{ij} = \langle \xi_i \xi_j \rangle$ and $\tilde{C}(t)$, vorticity and average probability angular momentum $\langle \mathcal{L} \rangle^*$. Since the bimodal probability density $P^*(\vec{\xi})$ is dominated by the peak $\vec{x}^{(+)}$ in the low-zealotry phase, the LGA is expected to work even better when the zealotry is asymmetric since the skewness that characterizes $P^*(\vec{\xi})$ in this regime disappears when N is large enough.

When the zealotry is asymmetric the long-time dynamics is characterized by metastability: While in principle

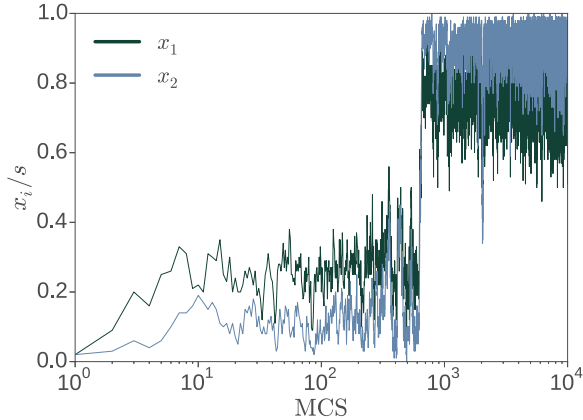


FIG. 12. (Color online). Metastability and switching dynamics in the low-zealotry phase with asymmetric zealotry: Shown is the first 10^4 MCS of a typical single realization with initial condition $\vec{x} = (0, 0)$ and switching occurring around $t \approx 1000$. Parameters are: $(N, S_1, S_2, Z_+, Z_-, q_1, q_2) = (258, 100, 100, 30, 28, 1, 2)$.

chance fluctuations can cause the continuous switching of susceptibles population from the (metastable state) $\vec{x}^{(-)}$ into the state $\vec{x}^{(+)}$ and vice versa, owed to the asymmetry in P^* only the switch from $\vec{x}^{(-)}$ to $\vec{x}^{(+)}$ is observable in practice (when $Z_+ > Z_-$). As in the q VMZ [16]. This phenomenon is associated with the metastability of the fixed points $\vec{x}^{(\pm)}$ and as such is triggered by a rare large fluctuation: As shown in Fig. 12, a chance fluctuation causes the sudden and almost simultaneous switch of both q_i -subpopulations from $\vec{x}^{(-)}$ to $\vec{x}^{(+)}$. In large population, the system settles in the new metastable and fluctuates in its vicinity but cannot be observed to switch back to $\vec{x}^{(-)}$. The mean time for the transition $\vec{x}^{(-)}$ to $\vec{x}^{(+)}$ can be estimated by using the same approach as in the case of symmetric zealotry and also gives a mean time that grows exponentially with the population size, which is typical of a system characterized by metastability.

VII. DISCUSSION AND CONCLUSION

This work has been dedicated to the detailed analysis of a heterogeneous out-of-equilibrium nonlinear voter model in a finite well-mixed population. More specifically, we have carefully analyzed the properties of $2q$ VZ model that we introduced in Ref. [17] where two types of swing voters need the consensus of q_1 or q_2 ($\neq q_1$) of its neighbors to adopt their opinion and are influenced by the presence of zealots. The $2q$ VZ is a direct but non-trivial generalization of the q -voter model with zealots (q VMZ) [16]. Both models mimic important concepts of social psychology and sociology, such as the relevance group-size on the mechanism of conformity for collective actions, and the interplay between independence and conformity. However, from a mathematical viewpoint the

$2q$ VZ strikingly differs from the q VMZ by violating the detailed balance and is therefore genuinely *out of equilibrium*. Many of the qualitative features of the $2q$ VZ are similar to those displayed by the q VMZ: When the zealotry density is low, the long-time opinion distribution is bimodal whereas it is single-peaked at high zealotry. Furthermore, the $2q$ VZ is also characterized by a switching dynamics when there is an equal number of zealots of both types and by metastability when there is an asymmetry in the zealotry. However, the non-equilibrium nature of the $2q$ VZ has far-reaching consequences that we have investigated in detail. In particular, we have characterized the system's non-equilibrium steady state (NESS) in terms of its probability distribution and probability currents that form closed loops in the state space, as well as the unequal-time correlation functions to highlight the violation of the time-reversal. These quantities have been computed numerically exactly for small systems and by means of stochastic simulations in larger populations. Furthermore, we have also investigated these quantities analytically in the realm of the linear Gaussian approximation (LGA) obtained in the limit of large systems and far from the criticality. We have also focused on the long-time switching dynamics of the $2q$ VZ in the low-zealotry phase and have devised an approximation by mapping the mean switching time of the $2q$ VZ on that computed in Ref. [16] for the q VMZ. We have also studied some properties of these systems at criticality and outlined the behavior of the $2q$ VZ the zealotry is asymmetric.

This work has allowed us to draw a comprehensive picture of the various properties of the $2q$ VZ and of the consequences of the violation of the detailed balance and we have shown that LGA is a particularly useful method. It shall be interesting to investigate this model on complex and/or adaptive networks that would be relevant from a social dynamics perspective. An intriguing question is the macroscopic interpretation of the closed loops of probability current: can these be related to the presence of “leaders” and “followers” in a society?

VIII. ACKNOWLEDGEMENTS

This work is supported by an EPSRC Industrial Case Studentship Grant No. EP/L50550X/1. Partial funding from Bloom Agency in Leeds U.K. is also gratefully acknowledged. We thank K Bassler, B Schmittmann and J B Weiss for enlightening discussions. This research is supported partly by US National Science Foundation grants OCE-1245944 and DMR-1507371. One of us (RKPZ) is grateful for the hospitality of the Leeds School of Mathematics, as well as financial support from the LSM and the London Mathematical Society (grant 41517). MM is grateful for the hospitality of the LSFrey at the Arnold Sommerfeld Center (University of Munich), as well as for the financial support of the Alexander von Humboldt Foundation (Grant No. GBR/1119205).

-
- [1] T. C. Schelling, *Am. Econ. Rev.* **59**, 488 (1969); *J. Math. Sociol.* **1**, 143 (1971); *Micromotives and Macrobbehavior* (WW Norton & Company, 1978).
- [2] C. Castellano, S. Fortunato, and V. Loreto, *Rev. Mod. Phys.* **81**, 591 (2009).
- [3] T. M. Liggett, *Interacting Particle Systems* (Springer, 1985) pp. 1–5.
- [4] S. Galam, *Sociophysics: a physicist's modeling of psycho-political phenomena* (Springer Science & Business Media, 2012); P. Sen and B. K. Chakrabarti, *Sociophysics: an introduction* (Oxford University Press, Oxford, 2013).
- [5] M. Granovetter, *Am. J. Sociol.* **83**, 1420 (1978).
- [6] B. Latané, *Am. Psychol.* **36**, 343 (1981); P. R. Nail, G. MacDonald, and D. A. Levy, *Psychol. Bull.* **126**, 454 (2000).
- [7] S. E. Asch, *Sci. Am.* **193**, 31 (1955); S. Milgram, L. Bickman, and L. Berkowitz, *J. Person. Soc. Psychol.* **13**, 79 (1969).
- [8] M. Mobilia, *Phys. Rev. Lett.* **91**, 028701 (2003); M. Mobilia and I. T. Georgiev, *Phys. Rev. E* **71**, 046102 (2005).
- [9] M. Mobilia, A. Petersen, and S. Redner, *J. Stat. Mech.* **2007**, P08029 (2007).
- [10] S. Galam and F. Jacobs, *Physica A* **381**, 366 (2007); K. Sznajd-Weron, M. Tabiszewski, and A. M. Timpanaro, *EPL* **96**, 48002 (2011); D. Acemoglu, G. Como, F. Fagnani, and A. Ozdaglar, *Math. Oper. Res.* **38**, 1 (2013); P. Nyczka and K. Sznajd-Weron, *J. Stat. Phys.* **151**, 174 (2013); E. Yildiz, A. Ozdaglar, D. Acemoglu, A. Saberi, and A. Scaglione, *ACM Trans. Econ. Comp.* **1**, 19 (2013); F. Palombi and S. Toti, *J. Stat. Phys.* **156**, 336 (2014); G. Verma, A. Swami, and K. Chan, *Physica A* **395**, 310 (2014); A. Waagen, G. Verma, K. Chan, A. Swami, and R. D'Souza, *Phys. Rev. E* **91**, 022811 (2015); D. L. Arendt and L. M. Blaha, *Comput. Math. Organ.* **21**, 184 (2015).
- [11] N. Masuda, *New J. Phys.* **17**, 033031 (2015); J. Xie, S. Sreenivasan, G. Korniss, W. Zhang, C. Lim, and B. K. Szymanski, *Phys. Rev. E* **84**, 011130 (2011); N. Masuda, *Sci. Rep.* **2** (2012); C. Borile, D. Molina-Garcia, A. Maritan, and M. A. Muñoz, *J. Stat. Mech.* **2015**, P01030 (2015); M. Mobilia, *Phys. Rev. E* **86**, 011134 (2012); *Chaos, Solitons & Fractals* **56**, 113 (2013); *Phys. Rev. E* **88**, 046102 (2013); *J. Stat. Phys.* **151**, 69 (2013); A. Szolnoki and M. Perc, *Phys. Rev. E* **93**, 062307 (2016).
- [12] C. Castellano, M. A. Muñoz, and R. Pastor-Satorras, *Phys. Rev. E* **80**, 041129 (2009).
- [13] F. Slanina, K. Sznajd-Weron, and P. Przybyła, *EPL* **82**, 18006 (2008); S. Galam and A. C. Martins, **95**, 48005 (2011); P. Przybyła, K. Sznajd-Weron, and M. Tabiszewski, *Phys. Rev. E* **84**, 031117 (2011); A. M. Timpanaro and C. P. Prado, **89**, 052808 (2014); A. M. Timpanaro and S. Galam, **92**, 012807 (2015); A. Jędrzejewski, A. Chmiel, and K. Sznajd-Weron, **92**, 052105 (2015); M. A. Javarone and T. Squartini, *J. Stat. Mech.* **2015**, P10002 (2015).
- [14] The version with $q = 2$ is closely related to the well-known models of K. Sznajd-Weron and J. Sznajd, *Int. J. Mod. Phys. C* **11**, 1157 (2000); F. Slanina and H. Lavicka, *EPJ B* **35**, 279 (2003); R. Lambiotte and S. Redner, *EPL* **82**, 18007 (2008).
- [15] In this work, we will ignore spatial structures, i.e., each voter is connected to every other, so that the term “neighbor” simply refers to any other individual in the population. Of course, to model reality more closely, we should study voters linked in more complex networks [40].
- [16] M. Mobilia, *Phys. Rev. E* **92**, 012803 (2015).
- [17] A. Mellor, M. Mobilia, and R. K. P. Zia, *EPL* **113**, 48001 (2016).
- [18] T. L. Hill, *J. Theor. Biol.* **10**, 442 (1966).
- [19] R. Zia and B. Schmittmann, *J. Stat. Mech.* **2007**, P07012 (2007).
- [20] R. Zia, J. B. Weiss, D. Mandal, and B. Fox-Kemper, in *Journal of Physics: Conference Series*, Vol. 750 (IOP Publishing, 2016) p. 012003 (See also arXiv:1610.02976)
- [21] M. Lax, *Rev. Mod. Phys.* **38**, 541 (1966).
- [22] J. B. Weiss, *Tellus A* **55**, 208 (2003); *Phys. Rev. E* **76**, 061128 (2007).
- [23] We have found the following typos in our Ref. [17]: Eq. (2) of [17] should read $W_i^-(\vec{n}) = \frac{n_i}{N} \left(\frac{Z-+S_1+S_2-n_1-n_2}{N-1} \right)^{q_i}$, and after Eq. (3) of [17], the quantity ρ should read $(1 - \mu^*)/\mu^*$.
- [24] A. Kolmogorov, *Math. Ann.* **112**, 155 (1936).
- [25] Henceforth, we denote quantities associated with the stationary state with * , unless explicitly stated otherwise.
- [26] Though a systematic procedure, given \mathcal{G} , to find P^* exists [18], it is too cumbersome to be practical in typical cases.
- [27] A. Mellor, M. Mobilia, and R. K. P. Zia, Figshare (2016), 10.6084/m9.figshare.2060595, (Supplementary Material).
- [28] M. S. Shkarayev and R. Zia, *Phys. Rev. E* **90**, 032107 (2014).
- [29] N. G. Van Kampen, *Stochastic Processes in Physics and Chemistry*, Vol. 1 (Elsevier, 1992); C. W. Gardiner *et al.*, *Handbook of Stochastic Methods*, Vol. 3 (Springer Berlin, 1985); H. Risken, *The Fokker-Planck Equation* (Springer, 1984).
- [30] N. Bogolubov and K. Gurov, *J. Exp. Theor. Phys.* **17**, 614 (1947); J. Yvon, *La théorie statistique des fluides et l'équation d'état*, Vol. 203 (Hermann & Cie, 1935).
- [31] For notational convenience, the variables in (15) are the averages $\langle \vec{x} \rangle$. There should be no confusion with components of \vec{x} in the configuration space.
- [32] If \mathbb{DF}^{-1} were symmetric, then detailed balance would be satisfied, which is not the case here.
- [33] In this subsection, we use Einstein's summation convention for repeated indices.
- [34] We have ignored the surface terms in the integration by parts here, which lies within the validity (and errors) of the Gaussian approximation.
- [35] To compare with LGA predictions in the low zealotry phase, we ensure that the trajectories never leave the vicinity of one of the two FPs. Naturally, these runs complement those we use for estimating switching times.
- [36] For example, the projection onto the ξ_1 -axis is given by $P^*(\xi_1) = \int_0^1 P^*(\xi_1, \xi_2) d\xi_2$.
- [37] P. Nyczka, J. Cisło, and K. Sznajd-Weron, *Physica A* **391**, 317 (2012).
- [38] H. Eyring, *J. Chem. Phys.* **3**, 107 (1935); H. A. Kramers, *Physica* **7**, 284 (1940); P. Hänggi, P. Talkner, and

- M. Borkovec, Rev. Mod. Phys. **62**, 251 (1990).
- [39] N. Goldenfeld, *Lectures on phase transitions and the renormalization group* (Addison-Wesley, Advanced Book Program, Reading, 1992); U. C. Täuber, *Critical dynamics: a field theory approach to equilibrium and non-equilibrium scaling behavior* (Cambridge University Press, 2014).
- [40] Y. Chuang, M. D’Orsogna, and T. Chou, Q. Appl. Math. (2016).

Appendix A: Master Equation and Probability Currents

In this appendix, we outline how the probability current is obtained from the master equation (ME) characterizing the evolution of a generic interacting stochastic process. For simplicity, let us focus on a system with configuration space $\{\mathcal{C}\}$, evolving in discrete time steps. Suppressing the reference to the initial configuration, \mathcal{C}_0 , we consider the evolution of $P(\mathcal{C}, t)$, the probability to find the system in the configuration \mathcal{C} at time t . In a general Markov chain with finite state space, this evolution is specified by only the probabilities for the system to transition from configuration \mathcal{C} to \mathcal{C}' in one time step: $W(\mathcal{C} \rightarrow \mathcal{C}')$. The ME for $P(\mathcal{C}, t)$ can be written as

$$P(\mathcal{C}', t+1) = \sum_{\mathcal{C}} \mathcal{G}(\mathcal{C}', \mathcal{C}) P(\mathcal{C}, t), \quad (\text{A1})$$

where the evolution operator \mathcal{G} thus reads

$$\mathcal{G}(\mathcal{C}', \mathcal{C}) = \delta(\mathcal{C}', \mathcal{C}) \left[1 - \sum_{\mathcal{C}''} W(\mathcal{C} \rightarrow \mathcal{C}'') \right] + W(\mathcal{C} \rightarrow \mathcal{C}'), \quad (\text{A2})$$

where δ is the Kronecker delta. Clearly, we can regard P as a vector and \mathcal{G} as a (stochastic) matrix, generating a new vector at each time step. The *change* in $P(\mathcal{C}, t)$ can be regarded as a sum over probability *currents* into and out-of \mathcal{C} . Specifically, the *net current* from \mathcal{C} to \mathcal{C}' is given by

$$K(\mathcal{C} \rightarrow \mathcal{C}', t) = W(\mathcal{C} \rightarrow \mathcal{C}') P(\mathcal{C}, t) - W(\mathcal{C}' \rightarrow \mathcal{C}) P(\mathcal{C}', t) \quad (\text{A3})$$

so that

$$P(\mathcal{C}, t+1) - P(\mathcal{C}, t) = - \sum_{\mathcal{C}'} K(\mathcal{C} \rightarrow \mathcal{C}', t) \quad (\text{A4})$$

takes the form of a discrete continuity equation. Much is known about stochastic matrices of the form \mathcal{G} . In particular, its largest eigenvalue is unity and there is (at least) one associated eigenvector, which can be identified with the stationary state, $P^*(\mathcal{C})$. Further, if the dynamics is ergodic (all \mathcal{C} ’s can be reached from any \mathcal{C}_0 with the W ’s), then P^* is unique.

Beyond probabilities at one time, we can consider joint distributions, with the system evolving from t to a later time $t + \tau$:

$$\mathcal{P}(\mathcal{C}', t + \tau; \mathcal{C}, t) = \mathcal{G}^\tau(\mathcal{C}', \mathcal{C}) P(\mathcal{C}, t) \quad (\text{A5})$$

where \mathcal{G}^τ is the matrix product of \mathcal{G} with itself, τ times.

If detailed balance is satisfied (i.e. if W ’s satisfy the Kolmogorov criterion [24]), then all currents in the stationary state

$$K^*(\mathcal{C} \rightarrow \mathcal{C}') = W(\mathcal{C} \rightarrow \mathcal{C}') P^*(\mathcal{C}) - W(\mathcal{C}' \rightarrow \mathcal{C}) P^*(\mathcal{C}') \quad (\text{A6})$$

vanish, yielding $K^* = 0$. When detailed balance is violated, then the stationary state is a NESS and some K^* will be non-vanishing. Stationarity implies that currents K^* are “divergence” free, i.e. $\sum_{\mathcal{C}'} K^*(\mathcal{C} \rightarrow \mathcal{C}') = 0$. This means that K^* must be the ‘curl’ of a certain quantity, while its ‘curl’ generally does not vanish. In other words, the currents form *closed loops* in \mathcal{C} space. By analogy with the current \vec{J} in classical mechanics of incompressible fluids (where $\vec{\nabla} \cdot \vec{J} = 0$), these current loops lead us to other concepts, notably the vorticity field ($\vec{\omega} = \vec{\nabla} \times \vec{J}$), the stream function ($\vec{J} = \vec{\nabla} \times \vec{\psi}$), and total angular momentum ($\int_{\vec{r}} \vec{r} \times \vec{J}$).

1. Probability Current and Observables in the 2qVZ

Here, we study discrete version of these quantities in a very simple configuration space: In the 2qVZ, the \mathcal{C} space is just the set of integer points $(n_1, n_2) \in S_1 \times S_2$. With (3), the evolution operator of the 2qVZ is given by (2). Hence, with (A3) and (3), the probability net current associated in the 2qVZ is given by

$$\begin{aligned} K_1(\vec{n}; t) &= W_1^+(\vec{n}) P(\vec{n}; t) \\ &\quad - W_1^-(\vec{n} + \vec{e}_1) P(\vec{n} + \vec{e}_1; t) \\ K_2(\vec{n}; t) &= W_2^+(\vec{n}) P(\vec{n}; t) \\ &\quad - W_2^-(\vec{n} + \vec{e}_2) P(\vec{n} + \vec{e}_2; t). \end{aligned} \quad (\text{A7})$$

In the continuum limit, $\vec{n}/N \rightarrow \vec{x}$, the usual notation of divergence and curl applies. Meanwhile, $\vec{K}^*(\vec{x}) = (K_1^*(\vec{x}), K_2^*(\vec{x}))$ is a two component vector field while both the vorticity and stream function are scalar fields:

$$\omega^*(\vec{x}) = \varepsilon_{ij} \frac{\partial K_j^*(\vec{x})}{\partial x_i}; \quad K_i^*(\vec{x}) = \varepsilon_{ij} \frac{\partial \psi(\vec{x})}{\partial x_j} \quad (\text{A8})$$

where ε_{ij} is the two-dimensional Levi-Civita symbol and repeated indices are summed. The interpretation of these quantities is the following: Vorticity ω^* represents the ‘essence’ or ‘source’ of \vec{K}^* , much like electric currents are the sources of magnetic field. On the other hand, \vec{K}^* is just a 90° rotation of $\vec{\nabla} \psi^*$ and ψ^* therefore provides a simple way to visualize the probability current.

Since it is generally difficult to visualize probability currents, it is also useful to introduce a quantity L_{ij} , which is the (average) “probability angular momentum” [17, 28] and the formal analog of the total angular momentum of a fluid:

$$L_{ij} = \int_{\vec{x}} \varepsilon_{ij} x_i K_j^*(\vec{x}) d\vec{x} = \int_{\vec{x}} [x_i K_j^*(\vec{x}) - x_j K_i^*(\vec{x})] d\vec{x}, \quad (\text{A9})$$

where $i, j \in (1, 2)$. The probability angular momentum has a single independent component, say $L_{12} = -L_{21} = \langle \mathcal{L} \rangle^*$. Since, \vec{K}^* is divergence-free ($\partial K_i / \partial x_i = 0$), $\langle \mathcal{L} \rangle^*$ is independent of the choice of the origin of $\{\vec{x}\}$.

We are particularly interested in the average number of q_i -susceptibles and their two-point correlation function in the NESS of the $2qVZ$, which read:

$$\begin{aligned} \langle n_i \rangle_T &= \sum_{\vec{n}} n_i P^*(\vec{n}), \\ \langle n'_i n_j \rangle_T &= \sum_{\vec{n}, \vec{n}'} n'_i n_j \mathcal{P}^*(\vec{n}, T; \vec{n}', 0). \end{aligned} \quad (\text{A10})$$

In particular, the lagged correlation $C_{ij}(\tau) = \langle x'_i x_j \rangle_T = \langle n'_i n_j \rangle_T / N^2$, is directly related to $\langle \mathcal{L} \rangle^*$ (A9) when $T = 1$. In fact, in continuous time $\tau \rightarrow t = T/N$, the average probability angular momentum $\langle \mathcal{L} \rangle^*$ is antisymmetric part $\tilde{C}_{ij} = C_{ij} - C_{ji}$ of this two-point unequal-time correlation function in the NESS [17]: $\langle \mathcal{L} \rangle^* = \partial_\tau \tilde{C}(\tau) \Big|_0$, see Eq. (32).

The proof for $\langle \mathcal{L} \rangle^* = \langle \vec{n} \times (\vec{W}^+ - \vec{W}^-) \rangle$ in NESS starts with

$$\langle \mathcal{L} \rangle^* = \sum_{\vec{n}} n_1 K_2^*(\vec{n}) - n_2 K_1^*(\vec{n})$$

and substituting in the expression for stationary flows (5). Rearranging various terms on the RHS we have

$$\begin{aligned} &= \sum_{\vec{n}} [n_1 W_2^+(\vec{n}) - n_2 W_1^+(\vec{n})] P^*(\vec{n}) \\ &\quad - \sum_{\vec{n}} n_1 W_2^-(\vec{n} + \vec{e}_2) P^*(\vec{n} + \vec{e}_2) \\ &\quad + \sum_{\vec{n}} n_2 W_1^-(\vec{n} + \vec{e}_1) P^*(\vec{n} + \vec{e}_1) \\ &= \sum_{n_1, n_2=0} n_1 W_2^+(n_1, n_2) P^*(n_1, n_2) \\ &\quad - \sum_{n_1, n_2=0} n_2 W_1^+(n_1, n_2) P^*(n_1, n_2) \\ &\quad + \sum_{n_1=1, n_2=0} n_2 W_1^-(n_1, n_2) P^*(n_1, n_2) \\ &\quad - \sum_{n_1=0, n_2=1} n_1 W_2^-(n_1, n_2) P^*(n_1, n_2) \end{aligned} \quad (\text{A11})$$

where $\sum_{n_1, n_2=0}$ is the sum over both indices, starting at 0. For the last two terms, we can sum over $n'_i = n_i + 1$ starting at $n'_i = 1$. But, since

$$W_1^-(0, n_2) = 0 = W_2^-(n_1, 0)$$

this sum can be extended to $n'_i \in [0, S_i]$.

$$\begin{aligned} &= \sum_{n_1, n_2=0} [n_1 W_2^+(\vec{n}_1, \vec{n}_2) - n_2 W_1^+(\vec{n}_1, \vec{n}_2)] P^*(n_1, n_2) \\ &\quad + \sum_{n_1, n_2=0} [n_2 W_1^-(\vec{n}_1, \vec{n}_2) - n_1 W_2^-(\vec{n}_1, \vec{n}_2)] P^*(n_1, n_2) \end{aligned}$$

Combining everything, we have

$$\langle \mathcal{L} \rangle^* = \sum_{\vec{n}} [n_1 (W_2^+ - W_2^-) - n_2 (W_1^+ - W_1^-)] P^*.$$

Appendix B: Calculating P^* for large systems

For small systems, the full master equation is solvable numerically to find the stationary state $P^*(\vec{n})$, and subsequently the stationary currents \vec{K}^* . This is very useful for assisting in the understanding of the model. However this approach is problematic in that the transition matrix $\mathcal{G} = [\mathcal{G}(\vec{n}', \vec{n})]$ grows in density exponentially in each power. As there are $(S_1 + 1) \times (S_2 + 1)$ possible states, the transition matrix has $(S_1 + 1)^2 (S_2 + 1)^2$ entries. For a systems with $S = (S_1 + S_2)/2 > 100$, storing these transition matrices fully in memory becomes non-trivial. For $S = 300$, the required memory is 65GB (with double precision) which is far beyond the realms of standard computer setups.

Thankfully it is possible to attain the stationary distribution for larger systems relatively quickly, managing a trade-off between computational intensity and memory. After computing the stationary distribution of a smaller system exactly we use linear interpolation to approximate the stationary distribution, $\tilde{P}^*(\vec{x})$, of a system which is a factor r larger (or a factor r more granular when considering the densities). In particular, for $r = 2$, we begin with

$$\tilde{P}^*(\vec{x}) = P^*(\vec{x})$$

for $x_i = n_i/N$ (and so $x_i = 2n_i/2N$). Then for the “missing points” we use the averages of their neighbours:

$$\tilde{P}^* \left(\frac{2n_i + 1}{2N}, \frac{2n_j}{2N} \right) = \frac{1}{2} \sum_{\eta=0,1} P^* \left(\frac{n_i + \eta}{N}, \frac{n_j}{N} \right)$$

for the i -direction, and similarly for the j -direction. Finally

$$\tilde{P}^* \left(\frac{2n_i + 1}{2N}, \frac{2n_j + 1}{2N} \right) = \frac{1}{4} \sum_{\eta, \kappa=0,1} P^* \left(\frac{n_i + \eta}{N}, \frac{n_j + \kappa}{N} \right)$$

We then use this approximate \tilde{P}^* as an initial distribution for further iteration. Since \tilde{P}^* closely resembles the actual stationary distribution, very few iterations are needed to reach good accuracy. This means that only lower powers of \mathcal{G} need to be calculated, alleviating possible memory issues for intermediate system sizes.

Appendix C: Calculating z_c and q_{eff} for arbitrary numbers of species

In the main text (Sec. V) we calculate the critical zealotry density z_c for a system consisting of two subpopulations, q_1 - and q_2 -susceptibles. For systems with symmetric zealotry ($z_{\pm} = z$) we are able to calculate z_c for a system with an arbitrary number N_s of subpopulations with a distribution q_i 's ($i = 1, 2, \dots, N_s$). Starting with the mean-field rate equations that are direct generalization of (15)

$$\frac{d}{dt}x_i = w_i^+ - w_i^- = (s_i - x_i)\mu^{q_i} - x_i(1 - \mu)^{q_i}. \quad (\text{C1})$$

where $\mu \equiv z_+ + \sum_{i=1}^{N_s} x_i$. The fixed points x_i^* of (C1) are given by

$$\frac{s_i}{x_i^*} = 1 + \rho^{q_i},$$

where $\rho \equiv (1 - \mu^*) / \mu^*$ satisfies

$$\mu^* = z_+ + \sum_{i=1}^{N_s} \frac{s_i}{1 + \rho^{q_i}} = \frac{1}{1 + \rho}.$$

We now specialize to the case of symmetric zealotry $z_{\pm} = z$. In this case, Eqs. C1 have always a fixed point $\vec{x}^{(0)} = (s_1/2, s_2/2, \dots, s_{N_s}/2)$ at the center for which

$$\rho = 1 \quad \text{and} \quad \mu^* = 1/2.$$

As in the case $N_s = 1, 2$ [16, 17], the generalized model exhibits criticality if $\vec{x}^{(0)}$ changes stability at some critical zealotry density z_c . The method for finding z_c follows as in the main text, exploiting the generalized stability matrix $\mathbb{F}(\vec{x}^{(0)}) = -[\partial \dot{x}_i / \partial x_j]_{\vec{x}^{(0)}}$

$$\begin{aligned} -\frac{\partial \dot{x}_i}{\partial x_j} \bigg|_{\vec{x}^{(0)}} &= -\frac{\partial [(s_i - x_i)\mu^{q_i} - x_i(1 - \mu)^{q_i}]}{\partial x_j} \bigg|_{\vec{x}^{(0)}} \\ &= -\delta_{ij} \left(\frac{1}{2}\right)^{q_i} + \frac{s_i}{2} q_i \left(\frac{1}{2}\right)^{q_i-1} \\ &\quad -\delta_{ij} \left(\frac{1}{2}\right)^{q_i} - \frac{s_i}{2} q_i \left(\frac{1}{2}\right)^{q_i-1} (-1) \\ &= 2^{1-q_i} [\delta_{ij} - s_i q_i] \end{aligned}$$

Now, $\det \mathbb{F}(\vec{x}^{(0)})$ is obtained from Sylvester's determinant theorem:

$$\det \mathbb{F}(\vec{x}^{(0)}) = 2^{N_s - \sum_i q_i} \left(1 - \sum_{i=1}^{N_s} s_i q_i\right)$$

so that, the criticality condition, $\det \mathbb{F}(\vec{x}^{(0)}) = 0$, yields

$$\sum_{i=1}^{N_s} s_i q_i = 1. \quad (\text{C2})$$

Hence, the critical zealotry density is $z_c = (1 - \sum_{i=1}^{N_s} s_i) / 2$ where the s_i and q_i 's are subject to satisfy (C2). As a result, it is the same as if we had a homogeneous population (i.e., $s_{\text{eff}} = \sum_{i=1}^{N_s} s_i$) with an effective $q = q_{\text{eff}}$ given by $s_{\text{eff}} q_{\text{eff}} = 1$. Thus, we find

$$q_{\text{eff}} = \frac{\sum_{i=1}^{N_s} q_i s_i}{\sum_{i=1}^{N_s} s_i},$$

which can easily be interpreted as the “average q ” of the population.

Appendix D: Explicit forms of \mathbb{C} & $\tilde{\mathbb{C}}(t)$ in the LGA

In this appendix we show how to compute the correlation matrix \mathbb{C} used in the realm of the linear Gaussian approximation (LGA) of section IV and give its explicit expression in the symmetric case ($Z_+ = Z_- = Z$ and $S_1 = S_2 = S$) with $q_1 = 1$ and $q_2 = 2$. We also outline the LGA calculation of $\tilde{\mathbb{C}}(\tau)$, the antisymmetric part of the unequal-time correlation function $C_{ij}(t) = \langle x_i(t + t_0) x_j(t_0) \rangle$ in the NESS (when $t_0 \rightarrow \infty$).

1. Explicit form of \mathbb{C} within the LGA

As explained in Sec. IV, in the realm of the LGA the stationary probability about a fixed point \vec{x}^* is given by $P^*(\vec{\xi}) \propto \exp\left[-\frac{1}{2}\vec{\xi} \cdot \mathbb{C}^{-1}\vec{\xi}\right]$, where $\vec{\xi} = \vec{x} - \vec{x}^*$ and $\mathbb{C} = [C_{ij}]$, $i, j = 1, 2$ is the symmetric real correlation matrix. The stationary probability density current within the LGA is $\vec{K}^* = -(\mathbb{F}\mathbb{C} - \mathbb{D})\mathbb{C}^{-1}\vec{\xi} P^*(\vec{\xi})$, where \mathbb{F} is the stability matrix. Since K^* is divergence-free, $\mathbb{F}\mathbb{C} - \mathbb{D}$ has to be antisymmetric and we thus have [19, 22]

$$\mathcal{S}(\mathbb{F}\mathbb{C}) = \mathbb{D}, \quad (\text{D1})$$

where $\mathcal{S}(\mathbb{F}\mathbb{C}) = (\mathbb{F}\mathbb{C} + \mathbb{C}\mathbb{F}^T)/2$ is the symmetric part of $\mathbb{F}\mathbb{C}$. Since the matrices \mathbb{F} and \mathbb{D} are thus readily obtained as explained in the main text, the expression of the correlation matrix is obtained by solving (D1). It is useful to remind the reader that in the main text, see Eq. (28), we have shown that $\mathbb{L} = [L_{ij}] = 2\mathcal{A}(\mathbb{F}\mathbb{C})$ where $\mathcal{A}(\mathbb{F}\mathbb{C}) = (\mathbb{F}\mathbb{C} - \mathbb{C}\mathbb{F}^T)/2$ is the antisymmetric part of $\mathbb{F}\mathbb{C}$ and \mathbb{F} is the stability matrix around \vec{x}^* (see also Refs. [17, 28]).

In the symmetric case $Z_+ = Z_- = Z$ and $S_1 = S_2 = S$, with $q_1 = 1$ and $q_2 = 2$, the explicit expressions of \mathbb{F} and \mathbb{D} around each fixed point are given in [27]. With those quantities, we find the following expressions of the covariance matrix:

-Around the fixed point $\vec{x}^{(0)}$ (with $s < 1/3$):

$$\mathbb{C}^{(0)} = \frac{s}{4N(1-3s)(3-4s)} \quad (\text{D2})$$

$$\times \begin{pmatrix} 3-10s+6s^2 & 2s(2-3s) \\ 2s(2-3s) & 3-7s+6s^2 \end{pmatrix}. \quad (\text{D3})$$

With this expression and that of the stability matrix $\mathbb{F}^{(0)}$ around $\vec{x}^{(0)}$ [27], the average probability angular momentum in the LGA is $L_{12} = \langle \mathcal{L} \rangle^* = \frac{s^2}{2N(3-4s)}$.

-Around the fixed points $\vec{x}^{(\pm)}$ (with $z < z_c = 1/6$):

$$C_{11}^{(\pm)} = \frac{2z(1-2z)(3-11z-24z^2-36z^3)}{N(6z-1)(3+2z)(1+2z)^2} \quad (\text{D4})$$

$$C_{22}^{(\pm)} = \frac{6z^2(1+2z)}{N(6z-1)(3+2z)} \quad (\text{D5})$$

$$C_{12}^{(\pm)} = C_{21}^{(\pm)} = \frac{2z^2(12z(1+z)-5)}{N(1+2z)(3+2z)(6z-1)}. \quad (\text{D6})$$

With the expression of $\mathbb{C}^{(\pm)}$ and the stability matrix $\mathbb{F}^{(\pm)}$ around $\vec{x}^{(\pm)}$ (see [27]), the probability angular momentum in the LGA is $\langle \mathcal{L} \rangle^* = \frac{4z^2}{N(3+2z)}$.

2. Calculation of $\tilde{\mathbb{C}}(t)$ within the LGA

In the realm of the LGA, the covariance matrix $\mathbb{C}(t)$ for a NESS around a given FP is explicitly given by

$\mathbb{C}\exp(-\mathbb{F}^T t)$, where $\mathbb{C} = \mathbb{C}(0)$ is obtained as described above and \mathbb{F} is the stability matrix. To obtain the anti-symmetric quantity $\tilde{\mathbb{C}}(t) = e^{-\mathbb{F}^T t} \mathbb{C} - \mathbb{C} e^{-\mathbb{F} t}$, we exploit Sylvester's formula to write

$$e^{-\mathbb{F} t} = \left(\frac{\lambda_+ e^{-\lambda_- t} - \lambda_- e^{-\lambda_+ t}}{\lambda_+ - \lambda_-} \right) \mathbb{I} + \left(\frac{e^{-\lambda_+ t} - e^{-\lambda_- t}}{\lambda_+ - \lambda_-} \right) \mathbb{F},$$

where \mathbb{I} is the identity matrix and $\lambda_{\pm} = \left(\text{Tr}\mathbb{F} \pm \sqrt{(\text{Tr}\mathbb{F})^2 - 4\det\mathbb{F}} \right) / 2$ are the eigenvalues of \mathbb{F} . Thus,

$$\tilde{\mathbb{C}}(t) = \left(\frac{e^{-\lambda_- t} - e^{-\lambda_+ t}}{\lambda_+ - \lambda_-} \right) \underbrace{[\mathbb{F}\mathbb{C} - \mathbb{C}\mathbb{F}^T]}_{=\mathbb{L}}. \quad (\text{D7})$$

Since $\tilde{\mathbb{C}}(t)$ is antisymmetric, it has only one independent quantity, say $\tilde{C}_{12}(t) = \tilde{\mathbb{C}}(t)$, and with the probability angular momentum $\langle \mathcal{L} \rangle^* = L_{12}$, we find explicitly $\tilde{C}(t) = \langle \mathcal{L} \rangle^* \left(\frac{e^{-\lambda_- t} - e^{-\lambda_+ t}}{\lambda_+ - \lambda_-} \right)$. For the symmetric case $S_1 = S_2 = S$ and $Z_+ = Z_- = N - 2S$ with $q_1 = 1$ and $q_2 = 2$, the eigenvalues λ_{\pm} are readily obtained from the explicit expressions of \mathbb{F} given in [27].